

ALTERATION AND GEOCHEMISTRY OF THE  
MONROE KNOWN GEOTHERMAL RESOURCE AREA

by

Charles David Miller

A thesis submitted to the faculty of the  
University of Utah in partial fulfillment of the requirements  
for the degree of

Master of Science

in

Geology

Department of Geology and Geophysics

University of Utah

December 1976

THE UNIVERSITY OF UTAH GRADUATE SCHOOL

SUPERVISORY COMMITTEE APPROVAL

of a thesis submitted by

Charles David Miller

I have read this thesis and have found it to be of satisfactory quality for a master's degree.

8/23/76

Date

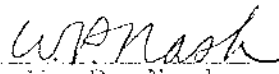
  
W. T. Parry

Chairman, Supervisory Committee

I have read this thesis and have found it to be of satisfactory quality for a master's degree.

8/23/76

Date

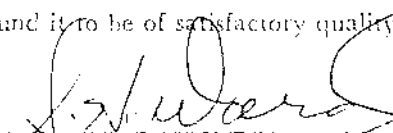
  
W. P. Nash

Member, Supervisory Committee

I have read this thesis and have found it to be of satisfactory quality for a master's degree.

8/24/76

Date

  
S. H. Ward

Member, Supervisory Committee

THE UNIVERSITY OF UTAH GRADUATE SCHOOL

FINAL READING APPROVAL

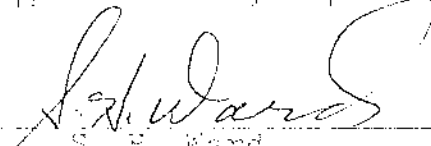
To the Graduate Council of The University of Utah:

I have read the thesis of Charles David Miller in its final form and have found that (1) its format, citations, and bibliographic style are consistent and acceptable; (2) its illustrative materials including figures, tables, and charts are in place; and (3) the final manuscript is satisfactory to the Supervisory Committee and is ready for submission to the Graduate School.

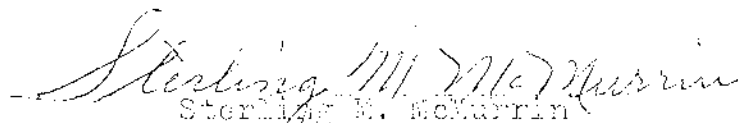
8/23/76  
Date

  
W. T. Parry  
Member, Supervisory Committee

Approved for the Major Department

  
S. E. Ward  
Chairman/Dean

Approved for the Graduate Council

  
Sterling M. McMurrin  
Dean of the Graduate School

## ACKNOWLEDGEMENTS

I would like to express my appreciation to Dr. William Parry who, in addition to being a good friend, has been an able advisor and a valuable resource in this study.

The computer software used in multivariate data analyses were furnished by Drs. Wayne Peeples and Allan Ekdale of the Department of Geology and Geophysics.

I would also like to express my appreciation to Carleen Nutter for her patient assistance in computer programming, Richard Dedolph for the use of his mass transfer routine and to Nancy Benson who conducted atomic absorption analyses on Monroe Spring waters.

## TABLE OF CONTENTS

	<u>Page</u>
ACKNOWLEDGEMENTS. . . . .	iv
LIST OF ILLUSTRATIONS . . . . .	vii
LIST OF TABLES. . . . .	ix
ABSTRACT. . . . .	x
INTRODUCTION. . . . .	1
Purpose and Scope . . . . .	1
Geological Setting . . . . .	1
Relationship to Other Utah KGRA's . . . . .	5
Previous Work. . . . .	5
GEOLOGY OF THE MONROE KGRA. . . . .	9
Methods. . . . .	9
Stratigraphy . . . . .	9
Spring Deposits. . . . .	17
Structure . . . . .	18
Alteration . . . . .	21
PETROGRAPHY . . . . .	25
Methods. . . . .	25
Major Minerals Occurring in the Monroe KGRA. . . . .	26
Primary phases . . . . .	26
Secondary phases . . . . .	27
Common Primary Textures. . . . .	39
Alteration Assemblages . . . . .	43
MULTIVARIATE ANALYSIS OF ROCK ALTERATION. . . . .	46
Methods. . . . .	46
Principle Component Analysis . . . . .	47
R Mode Cluster Analysis. . . . .	54
Q Mode Cluster Analysis. . . . .	62
SPRING GEOCHEMISTRY . . . . .	72
Methods. . . . .	72
Calculation of Ion Activities. . . . .	75

Table of Contents  
Continued

	<u>Page</u>
Origin of the Monroe Spring Water. . . . .	76
Heat Flow. . . . .	90
ALTERATION GEOCHEMISTRY . . . . .	93
CONCLUSION. . . . .	108
APPENDIX. . . . .	110
Data From Bulk Rock, Clay Fraction XRD and Thin Sections . . . . .	110
Data From Bulk Rock and Clay Fraction XRD Only. . . . .	112
Data From Bulk Rock XRD and Thin Sections Only. . . . .	113
Data From Bulk Rock XRD Only . . . . .	115
REFERENCES. . . . .	118
VITA. . . . .	121

## LIST OF ILLUSTRATIONS

<u>Figure</u>		<u>Page</u>
1	Index map of the Monroe area . . . . .	2
2	The locations of the Monroe, Sulphur- dale and Roosevelt KGRA's relative to important Tertiary volcanic formations. The major faults influencing these areas appear as dark lines . . . . .	6
3	Geologic map of the Monroe KGRA . . . . .	10
4	Alteration map of the Monroe KGRA . . . . .	12
5	Distribution of sulfate minerals, montmorillonite and biotite con- taining saganitic rutile . . . . .	37
6	R mode cluster of raw 30 x 15 array . . . . .	55
7	Abundances, reported in percent pattern intensity, of four alteration minerals versus plagio- clase and kaolinite . . . . .	58
8	Abundances, reported in percent pattern intensity, of five alteration minerals versus plagioclase, kaolinite, and carbonate . . . . .	60
9	Q mode cluster analysis of raw 95 x 15 array . . . . .	65
10	Histograms showing the distribution of phases among the three clusters chosen from cluster analysis of raw 95 x 15 array. Values of "volume percent" are percent pattern intensities . . . . .	67
11	Areal distribution of three clusters chosen from cluster analysis of raw 95 x 15 array . . . . .	69
12	Chloride and silica content of wells and springs in the Central Sevier River Valley. .	82

List of Illustrations  
(continued)

<u>Figure</u>		<u>Page</u>
13	Quartz saturation temperatures for wells and springs of the Central Sevier River Valley . . . . .	85
14	Proposed model for the Monroe Hot Springs . . . . .	88
15	Stability relations among the phases alunite, kaolinite, Ca-montmorillonite and microcline at 150°C for solutions saturated with respect to gypsum and quartz. . . . .	97
16	Stability relations among the phases alunite, kaolinite, Ca-montmorillonite and microcline at 60°C for solutions saturated with respect to gypsum and quartz. . . . .	99
17	Stability relations among the phases alunite, kaolinite, gibbsite, Ca-montmorillonite, muscovite and microcline as a function of temperature, pH and silica concentration. Saturation with gypsum is assumed. The calcite saturation line is shown for a PCO <sub>2</sub> of four atmospheres. The solution path is shown for the reaction of the proposed initial solution with potassium feldspar. . . . .	102



LIST OF TABLES

<u>Table</u>		<u>Page</u>
1	Principle axis factor loadings for the 30 x 15 data array. . . . .	49
2	Principle axis factor loadings for the 95 x 15 data array. . . . .	53
3	Warm spring waters in the Monroe area . . . .	74
4	Activities of aqueous species in the Red Hill Spring . . . . .	77
5	Activities of aqueous species in the Joseph Hot Springs. . . . .	78
6	Thermodynamic data. . . . .	94

## ABSTRACT

The Monroe known Geothermal Resource area is one of several active hot spring areas in south-central Utah. Associated with it is extensive hydrothermal alteration of Tertiary volcanic rocks. The major episode of alteration is of Pleistocene age and is associated with the northeast trending range front faults. An older episode is associated with north trending fractures and faults.

The spring water is derived from the mixing of hot, acid sulfate solutions with local groundwaters. The chemistry of these springs is consistent with the alteration assemblages in the area. The temperature of mixing for the spring waters and altering fluids has never much exceeded 150°C. The minimum temperature estimate for the present day hot source solutions is 100°C. Due to the thick carbonate sedimentary rock which immediately underlies the spring area, the system is profoundly affected by carbonate equilibria.

The theoretical heat flow anomalies associated with the proposed spring model have been estimated. Thermal gradients which are roughly twice and three times the average normal gradient for this region are anticipated over the plateau lands east of the springs and over the range front, respectively.

A semi-quantitative approach, applicable to reconnaissance studies, was applied to the interpretation of the exposed alteration. The relative abundances of minerals were estimated by x-ray diffraction techniques and the resulting data were evaluated via principle component analysis and cluster analysis. This procedure has proven successful at Monroe, where alteration assemblages are poorly developed and the zonal patterns obscure.

A zonal pattern of alteration has been recognized in which a kaolinite-jarosite assemblage passes outward to a kaolinite-mixed layer assemblage and finally to a montmorillonite-mixed layer clay assemblage. Carbonate is abundant throughout the area.

## INTRODUCTION

### Purpose and Scope

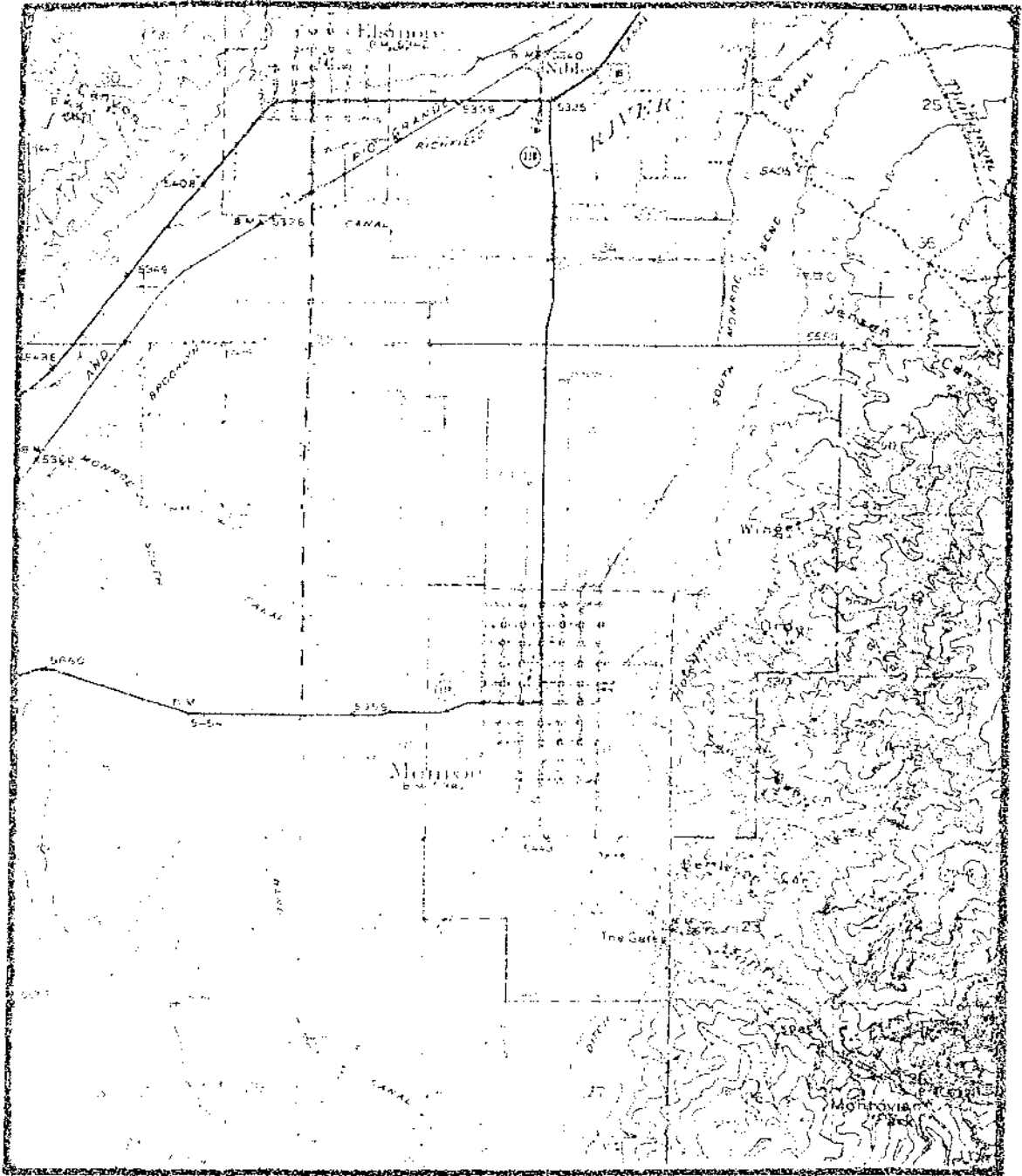
The Monroe Hot Springs known Geothermal Resource Area (KGRA) was chosen for a detailed alteration study on the basis of accessible thermal waters, high Na-K-Ca wall rock equilibration temperatures and extensive hydrothermal alteration which is exposed in nearly 1,000 feet of relief. The petrology and geochemistry of the surficial alteration were examined in order that boundary conditions might be established for the temperature and composition of the altering fluids. The characteristic pattern of alteration associated with this area was also studied so that it might be compared with the alteration prevalent in other proven and prospective geothermal resources.

### Geological Setting

The Monroe KGRA occupies the eastern flank of the Central Sevier River Valley, immediately to the east of the town of Monroe, Utah (fig. 1). Warm springs and seeps outcrop for approximately a mile, both north and south of Monroe.

The Central Sevier River Valley is bounded to the east by the steep, deeply dissected monocline of the Sevier Plateau and to the west by the Pavant Range. The

Figure 1. Index map of the Monroe area.



Antelope Range, a series of low hills, crosses the valley about ten miles south of Monroe.

The Bullion Canyon volcanics of Miocene age comprise the oldest volcanic rock in the area. They are composed of pyroclastics in the lower part, which are overlain by thick porphyritic latite flows. The total thickness is estimated at 4,000 feet (Callaghan & Parker, 1961).

Latite, basaltic andesite and rhyolite of the Dry Hollow, Joe Lott and Mount Belknap formations, all of Pliocene age, overlie the Bullion Canyon volcanics.

Quartz monzonite intrudes the Bullion Canyon volcanics at Monrovia Park, three miles southeast of Monroe. This stock, about one mile in diameter, is typical of other Miocene intrusives that have invaded the Bullion Canyon volcanics in the Marysvale district.

Tertiary volcanics are underlain by sedimentary rocks. The Jurassic formation, an equivalent of the Arapahoe shale, locally underlies the Bullion Canyon volcanics and is composed of stratified salts, lenticular gypsum beds and thin bedded limestones and shales. This formation attains a maximum thickness of 2,500 feet in the Central Sevier River Valley between Gunnison and Richfield before it disappears under the Tertiary volcanic cover (Hardy, 1952).

This region is typified by high angle normal faulting. The Sevier fault, from which the warm springs issue, terminates the west dipping monocline of the Sevier Plateau. The trace of this fault is mostly buried beneath alluvium.

Other major range front faults in this locality are the Elsinor fault and the Dry Hollow fault, which is associated with the Joseph Hot Springs area. The Antelope Range is the expression of an anticlinal cross-structure which extends eastward from the Tushar Mountains and terminates against the Sevier fault.

Several major landslides have formed along the shoulder of the Sevier Plateau. The largest of these is the Thompson Creek Slide which involves the Dry Hollow formation immediately adjacent to the Monroe KGRA.

#### Relationship to Other Utah KGRA's

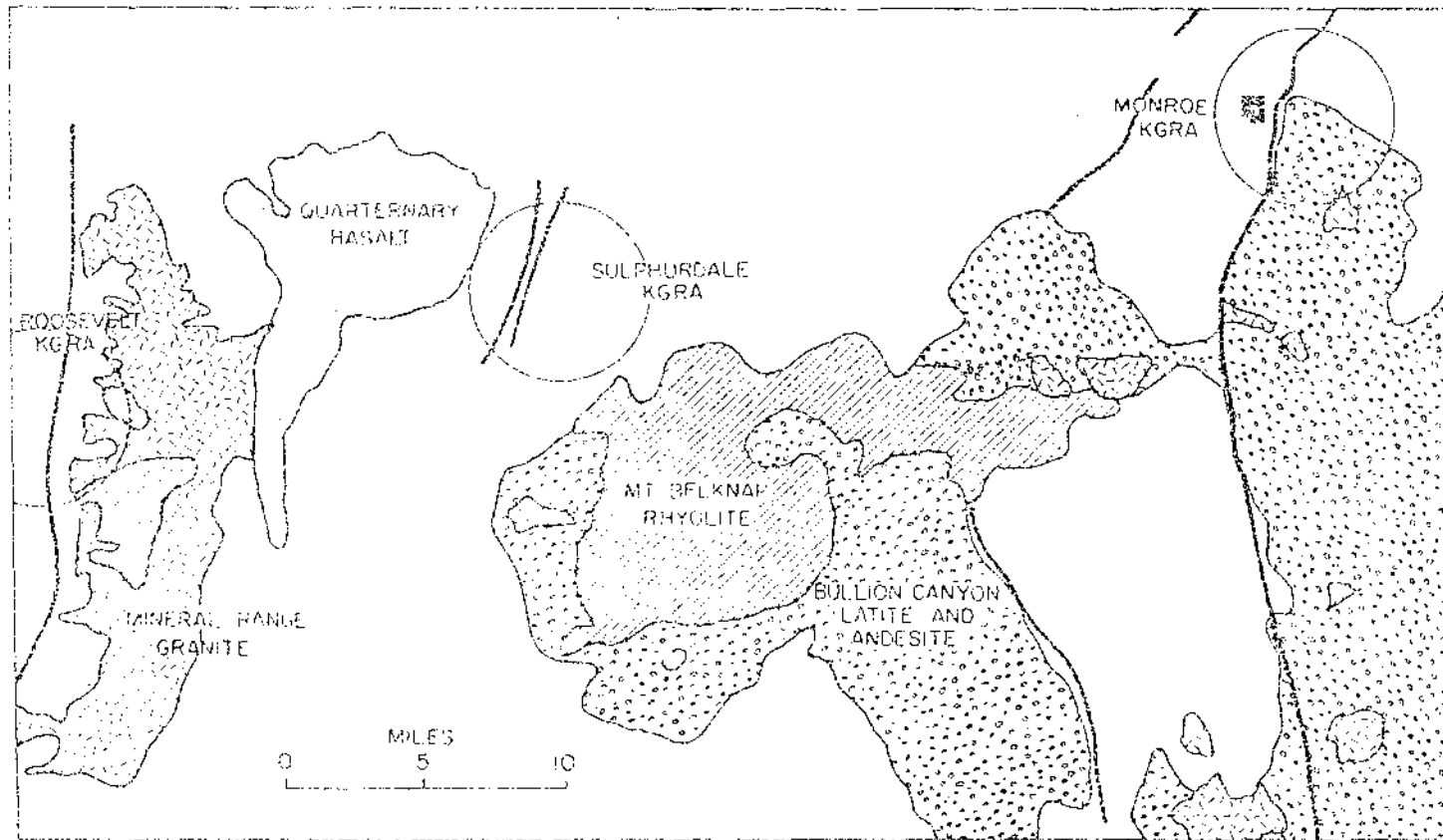
Figure 2 shows the position of the Monroe KGRA relative to the Sulphurdale and Roosevelt Hot Springs KGRA's. The linear arrangement of these three areas may reflect a major deepseated cross-structure which is associated with mineralization and hydrothermal activity in central Utah. The youngest silicic volcanic rocks outcrop in the vicinity of the Roosevelt Hot Springs KGRA; however late Tertiary rhyolitic activity is typical of the entire region. The Mount Belknap rhyolite is the most extensive of these acid volcanics.

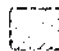
#### Previous Work


Callaghan and Parker (1961) mapped the geology of the Monroe quadrangle which includes all of the area within the Monroe KGRA. They recognized three mappable units within the Bullion Canyon volcanic formation. They did not,





Figure 2. The locations of the Monroe, Sulphurdale and Roosevelt KGRA's relative to important Tertiary volcanic formations. The major faults influencing these areas appear as dark lines.



 RHYOLITE

 BASALT

 LATITE AND ANDESITE

 QUARTZ MONZONITE

however, differentiate the lower pyroclastic sequence. The stratigraphy and mineralization of the Marysvale volcanic sequence has been described in two papers (Callaghan, 1938 and 1939).

## GEOLOGY OF THE MONROE KGRA

### Methods

An area of three square miles adjacent to the Monroe and Red Hill Springs was mapped during a six week period in the late summer of 1975. Mapping was done on aerial photo base on a scale of 1:4800. General geology, hydro-thermal alteration, and sample locations were included in the map. This information was later transferred to a topographic base (U.S.G.S. topographic quadrangle). The geologic and alteration maps appear in figures 3 and 4, respectively.

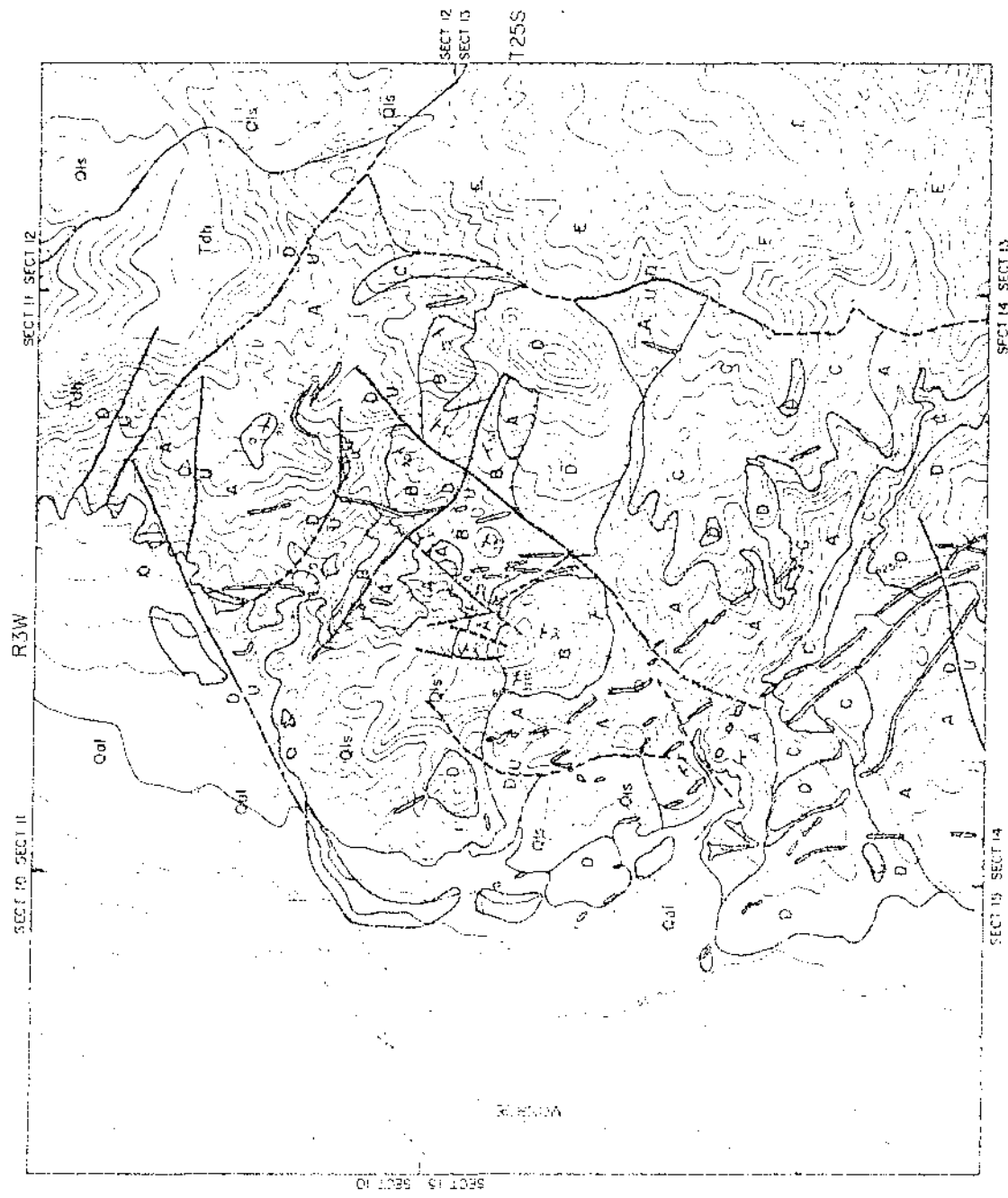
### Stratigraphy

The pyroclastic member of the Bullion Canyon formation which outcrops over most of the KGRA has been divided into four mappable lithologic units. The numbered locations of important outcrops in the following descriptions are referenced to figure 4.

Unit A is comprised of volcanic conglomerate, agglomerate, breccia, tuff and a few thin flows. The conglomerate contains angular to sub-angular heterogeneous pebbles and cobbles up to 15 centimeters in diameter. Fresh outcrops of a dark chocolate brown conglomerate are separated from leached light gray exposures by an irregular

Figure 3. Geologic map of the Monroe KGRA.

GEOLOGY BY CHARLES D MILLER  
1976



LEGEND

**Quaternary**

- Qal QUATERNARY ALLUVIUM
- Qis QUATERNARY LOESS
- Tdh TERTIARY DELTAIC SANDS

**SOIL BY CANYON VOLCANIC FORMATION**

- E EOLIAN SANDS
- D DUNE SANDS
- C CLAYEY SANDS
- B BROWN SANDS
- A ALLUVIUM

**MOIOCENE**

- INFERRED

**TERTIARY VOLCANICS**

- INFERRED

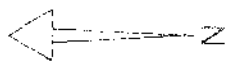
**Other Features:**

- ROAD
- RAILROAD
- WATER
- WELL
- POLE
- POST
- SHED
- HOUSE
- CHURCH
- SCHOOL
- STATION
- OFFICE
- FACTORY
- MINES
- QUARRY
- GRAVE
- CEMETERY
- CHURCH
- SCHOOL
- STATION
- OFFICE
- FACTORY
- MINES
- QUARRY
- GRAVE
- CEMETERY








**Scale:** 0 1000 2000 FEET

**North Arrow:** N

Figure 4. Alteration map of the Monroe KGRA.



LEGEND

-  INTERMEDIATE TO HIGH ALTITUDE
-  MOUNTAIN TO INTERMEDIATE ALTITUDE
-  LAKE BEDS
-  UNCLASSIFIED
-  RAILROAD
-  HIGHWAY
-  STREAM





contact resembling a solution boundary. This contact is clearly visible in Order Canyon (location 302). Clasts are frequently a bright green as a result of propylitic alteration. The conglomerate fractures across clast boundaries. It weathers into gentle slopes. The clastic texture may not be distinct on weathered surfaces. A thin bedded, arenaceous gray tuff, which intervenes in the conglomerate has been designated as unit "A" in figure 3.

Agglomerate lies above the conglomerate. It forms gray cliff faces and weathers into massive blocks. In Order Canyon it contains chocolate brown stringers and veinlets (location 118). In altered outcrops it may be indistinguishable from conglomerate. Agglomerate grades upward into coarsely brecciated flows. This breccia may be gray to rust colored and outcrops irregularly in narrow ledges.

Thin, dark reddish-brown porphyritic flows, from several centimeters up to one meter in thickness, intervene sporadically between the conglomerate and agglomerate (location 232).

A rust colored crystal tuff is irregularly exposed. It weathers into low hills and gentle slopes, but occasionally forms small ledges. It is considered to represent the uppermost horizon of unit A. Brecciated outcrops of this tuff are common (location 197).

Unit B is composed of interbedded tuff and volcanic conglomerate. The conglomerate is distinguished from that

of unit A by well rounded cobbles and boulders and by its distinct bedding which is frequently graded. It fractures along clast boundaries and the rounded cobbles tend to weather out of the matrix. The conglomerate is invariably gray in appearance and forms steep cliffs and ledges. Alternating with the conglomerate is a thin, bedded, arenaceous gray tuff which is indistinguishable from the gray tuff in unit A. Channel fill structures are common among these tuffs and conglomerates. Due to its pronounced bedding, this unit afforded the only reliable measurements of attitudes in the area. The best exposures are available on 'SS' Mountain east of the Monroe spring.

Unit C is a dark purplish gray porphyritic latite flow, believed to be identical to Callaghan's Monrovia Latite member (Callaghan & Parker, 1961). It forms prominent shelves and tables in the southern part of the KGRA. It attains a maximum thickness of approximately 50 meters in Sand Canyon (location 51). Broad scree slopes generally lead up to well jointed outcrops. Weathered surfaces may look brown as a result of oxidation. The flows grade continuously into aphanitic dikes.

Unit D is a massive, pink to light purple crystal tuff. It is distinguished from the crystal tuff of unit A by containing accidental fragments of dark brown flows and peculiar white patches, presumably the relic outlines of lapilli. Large biotite phenocrysts may give the rock a salt and pepper appearance. This tuff forms steep hills

and rounded cliffs and weathers into large massive blocks.

Doloritic and aphanitic dikes outcrop in all four pyroclastic units. All dikes appear to be cogenetic with the porphyritic latite of unit C. The most conspicuous doloritic dikes have been sampled at locations 1, 13, 39, 20, 22 and 6. All weather to a light tan and many, particularly the aphanitic dikes, are markedly foliated. "Picture rock" type staining is common in intensely altered zones and the townspeople frequently use dike rock, so altered, for decoration. Aphanitic latite observed at locations 39, 22 and 20 apparently represents the chilled margins of the doloritic dike with which it occurs. As a rule, aphanitic dikes are no more than a meter in width while doloritic dikes are 5 meters wide or better. All dikes trend north to northwest and dip at angles of 30 to 35° to the east and northeast. It is, perhaps, more than a coincidence that a dike intersects each one of the active spring sites. Possibly, the dikes occupy fractures which continue to be important fluid pathways.

A rust colored porphyritic latite flow, Callaghan's Calcic Latite member (Callaghan & Parker, 1961), which outcrops to the east of the pyroclastic member of the Bullion Canyon volcanics has been designated unit E. In this locality the Calcic Latite can be distinguished from the Monrovia Latite by its deep rust color and by its more coarsely porphyritic texture. It forms broad ridges with gentle slopes which are generally littered with fine skree.

The only other formation which outcrops in the area is the Dry Hollow formation. In this locality it is comprised of dark brown porphyritic andesite flows. It can be distinguished from the Calcic Latite only with difficulty. The Dry Hollow formation forms a steep cliff at the northern edge of the area.

The pyroclastic units vary dramatically in thickness across the KGRA and often rest disconformably upon one another. The implication is that most, if not all, the pyroclastic units were deposited on an irregular terrain. In particular, the porphyritic latite of unit C appears to have flowed along old drainages. A striking disconformity between units A and D located east of 'SS' Mountain testifies to the degree to which the terrain was dissected at the time of the deposition of the massive crystal tuff. In addition, the peculiar conglomerates and tuffs of unit B, whose clasts have the appearance of alluvially worked sediments, projects a youthful terrain.

A small outcrop of unsorted and poorly consolidated conglomerate outcrops at location 192. It contains extremely angular clasts of volcanic rock, some of which approach 30 centimeters in diameter. From all appearances this is a very young conglomerate and probably belongs to the Sevier River formation.

#### Spring Deposits

With the exception of intermittant warm spring seeps,

the warm springs in the vicinity of Monroe are confined to two large tufa mounds. Red Hill Spring issues from a fissure in the northern-most and smaller of these mounds. It possesses the highest temperature and flow rate of any spring in the area. The flow, which is strong and constant, has been estimated at 200 gallons per minute (Mundorf, 1970). The Monroe mound is over 500 meters in length and contains myriad transient springs and seeps. The total flow from the mound, however, is comparable with the Red Hill Spring. The owner of the property has trenched the mound to increase and direct the flow. The temperatures of these springs varies between  $48^{\circ}$  and  $69^{\circ}\text{C}$ , compared to  $77^{\circ}\text{C}$  at Red Hill Spring. Intermittant seeps outcrop at all the tufa deposits along the range front. The ground in these areas is often warm, even when there is no visible flow. Ground temperatures as high as  $35^{\circ}\text{C}$  were measured at the mouth of Sand Canyon.

#### Structure

All hydrothermal alteration is confined to the pyroclastic member of the Bullion Canyon volcanic formation. The major faults which bring these rocks into contact with the Calcic Latite member and the Dry Hollow formation terminate the thermal area on the east and north, respectively. Together these two faults define a block, containing the pyroclastics, which is displaced upward relative to the adjacent terrain. This block is charac-

terized by intense fracturing and closely spaced en echelon normal faults. In many cases it was impossible to elucidate these detailed structures. Wherever displacements are apparent, faults have been mapped. These traces, while not in and of themselves sufficient to reconcile all the geology, are adequate to characterize the pattern of faulting in the KGRA.

Three sets of faults and fractures can be generalized; one trending northwest, a second northeast and a third north. The first two sets are responsible for the significant displacements in the area. The patterns of hydrothermal alteration, however, are controlled by the latter two sets. In the vicinity of the Red Hill Spring and throughout the central part of the area, travertine veins and fractures have a remarkably uniform north trend and dips of between 30 and 40°. At Red Hill Spring the most intense alteration occurs at the intersection of west dipping fractures and the major northeast trending faults. En echelon faults at location 175, near the spring, dip 30° to the east. The distribution of hydrothermally altered outcrops between locations 187 and 82 highlights a well developed set of north trending fractures. The aphanitic dikes in this area also reflect this local fracture pattern.

In the southern half of the area the north trending fractures dwindle to insignificance and northeast trending fractures dominate. The most extensive alteration found in the KGRA occurs in this region. Here the dikes, many

of which are doleritic, do not follow the local fractures but dip to the northeast. In Berthelson Canyon, south of the mapped area and separated from it by a major fault, northwest trending fractures become important in controlling hydrothermal alteration. Despite the changing trends in structure, the Bullion Canyon volcanics appear to maintain a reasonably uniform southwestern dip between Order and Monrovia Canyons.

The regions mapped as Quaternary landslide (Qls) on the range front are disrupted outcrops of units A and B. This rock is apparently draped over hidden range-front faults. Slumping of large volumes of this rock has produced chaotic attitudes and contacts in these areas. Travertine veins are densely distributed in this confused terrain. An arcuate trace represents the inferred range fault(s) associated with this structure.

Large slump blocks of unit B occur on the slope south of location 202. The clusters of tilted junipers which have grown from these blocks testify that this is a contemporaneous feature.

The massive Thompson landslide, which occupies the Dry Hollow formation, outcrops at the extreme northeastern corner of the KGRA. It has little bearing upon the structure or geology of the area.

The Miocene intrusive episode that resulted in the emplacement of the quartz monzonite stock at Monrovia Park may have generated the north and northwest trending

fractures and faults. These structures are arranged radially with respect to the Monrovia Park stock and many of them are occupied by latite dikes. In addition, the north trending fractures and faults do not conform to the present day topography. The structural complexity of the central part of the area may be the result of the intrusion of a stock at depth beneath the KGRA.

According to Callaghan & Parker (1961) the onset of range front faulting is contemporaneous with the deposition of the Sevier River formation which is late Pliocene or Pleistocene in age. The most intense alteration is confined to these northeast trending faults and fractures. Therefore, the beginning of the major hydrothermal episode is presumed to have been within the last several million years. The thermal system may not have changed significantly and the present day spring geochemistry might reasonably be expected to reflect the geochemistry of the recent past.

#### Alteration

The most striking aspect of the alteration within the KGRA is yellow, earthy patches that stand out against the light purple to light gray volcanic host rock. The nearly total involvement of the rock in the southwest corner of the area is clearly visible from the town of Monroe. These patches are generally distributed in distinct linear patterns and for the most part trend northeast, following



the major range front faults. The patches are characterized by white, tan and yellow mottling and invariably contain dendritic veins of gypsum. Large euhedral selenite crystals can commonly be collected from the weathered soils. Calcite veins are less common but are, nonetheless, a frequent feature of these areas. Primary textures may be partially or completely obscured by kaolinite and calcite replacement. The rock is usually banded by hematite stain. The enclosing gray to purple rock shows little variation, except in color from the patches. It is usually punky and foliated, like the patches, and frequently has undergone extensive carbonate or kaolinite replacement. Aphanitic dikes are generally more resistant than doleritic dikes when involved by this alteration. Where large patches do not occur yellow bands, several centimeters to one meter in width may surround fractures.

Yellow patches and bands may be the expression of either argillic or advanced argillic alteration, for these two are indistinguishable in outcrop. There is a tendency for argillic outcrops to be more weather resistant and to contain more vein calcite. These criterion are not to be trusted, however.

Less common but more dramatic are argillically altered outcrops which are distinguishable by their bright red, black and white coloration. These outcrops are confined to the northern half of the area and are most common along the fault connecting locations 128 and 139. Rock so

altered is an aggregate of quartz, kaolinite and iron oxide. It is unresistant to weathering and is found in deeply dissected exposures. A good example of this alteration is available at location 187. The Red Hill tufa mound, which takes its name from the bright red imparted by contained hematite, appears to be genetically related to these outcrops.

Propylitically altered rock can, in some cases, be recognized by the bright green specks or patches it contains. The green is not produced by chlorite but by montmorillonite, presumably the variety nontronite. Occasionally, propylitic outcrops may be indistinguishable from those of argillic zones. Also, many of the freshest outcrops in this area contain propylitic mineral assemblages. In any case, propylitic alteration is not well developed in this area.

A general pattern of alteration can be discerned in which iron argillic assemblages are associated with north-south structures while sulfate dominated argillic assemblages are associated with northeast-southwest structures. Implied in this pattern is the possibility that the iron rich hydrothermal solutions may have anteceded the sulfate solutions.

The hydrothermal alteration at Red Hill Spring is characterized by west dipping travertine veins, succeeded to the east by zones of kaolinite and calcite replacement.

The kaolinite replaced rock is tan to yellow and frequently contains masses of pure white kaolinite. The calcite replaced rock is gray and may contain specks of green montmorillonite. This rock usually has a salt and pepper appearance due to kaolinized andesine phenocrysts. Both zones are very earthy. Where this zonation is obscured by weathering, yellow soil containing abundant small selenite crystals outcrop instead. The flanks of the low hills adjacent to the spring are mantled by gray montmorillonitic "popcorn" alluvium. A similar but less distinct pattern of alteration occurs in the vicinity of Monroe Spring.

## PETROGRAPHY

### Methods

Hydrothermally altered areas as well as adjacent host rock were sampled and the sample locations recorded on the base map (figure 4). The specimens were then examined under a binocular microscope. Based on this examination a collection of 95 representative specimens was assembled. A 50 gram portion from each of these was pulverized in a Spex shatter box for four minutes. X-ray diffraction patterns were then made for powder pack mounts of each specimen. A Phillips Electronics diffractometer with a copper source and a graphite monochromator was used. Two-micrometer clay fraction mounts were also made by peptizing with calgon, separating the two micrometer fraction with a centrifuge, and smearing a centrifuged slurry on frosted glass slides. Thirty such preparations were made and x-ray patterns recorded for slides which were air dried, glycolated, dehydrated at 300°C, and heated to 700°C.

The composition of each of the 95 specimens was reported in terms of percent total pattern intensity attributable to the major peak of each phase. This semi-quantitative data were stored on a fastrand data file for use in multivariate data analysis. The data are reported

in appendices one through four.

Relying on the x-ray diffraction data, a representative group of 51 specimens was chosen to be made into thin sections. All sections were stained for potassium feldspar. If dolomite was present in the x-ray pattern of a specimen, dolomite was also stained. The sections were examined with a conventional petrographic microscope. Phases which had previously gone undetected by x-ray diffraction, but were recognized in thin section, were added to the data file nominally at one percent total pattern intensity.

#### Major Minerals Occurring in the Monroe KGRA

##### Primary Phases

Andesine. Andesine is the most frequently encountered plagioclase feldspar, with oligoclase or labradorite occurring in less than ten percent of the outcrops sampled. It appears both as large tabular phenocrysts in crystal tuff, agglomerate and porphyritic latite, and as small laths in the groundmasses of agglomerate, and porphyritic and aphanitic latites. Both Albite and Carlsbad twin laws are characteristic of the larger phenocrysts. Phenocrysts zoned toward alkali feldspar are common, the most extreme examples being andesines rimmed by potassium feldspar.

Andesine typically alters to calcite, kaolinite or montmorillonite. Occasionally sericite is also found

replacing andesine. As a rule the lathlike crystals alter much more readily. The larger phenocrysts alter from their interiors outward and frequently alkali feldspar rims will be preserved unaltered in otherwise kaolinized samples.

Apatite. Apatite occurs as euhedral hexagonal crystals and is found primarily in crystal tuff or porphyritic latite. It is commonly found as inclusions in fresh and altered biotite phenocrysts and appears to be closely associated with the occurrence of that mineral. It is unaltered in all specimens with the exception of 13II where it alters to gypsum. Both uniaxial and biaxial varieties were observed.

Biotite. Large tabular phenocrysts with perfect hexagonal cross-sections are abundant in crystal tuff. In agglomerate, however, biotite may appear as small clastic fragments and narrow laths. It is altogether absent from both porphyritic and aphanitic latites. In most specimens the biotite cleavages are warped or broken.

Hematite and carbonate frequently rim biotite phenocrysts even in the freshest outcrops. Biotite is most commonly replaced by montmorillonite, sericite or hematite. However, potassium feldspar also has been observed replacing biotite. Chlorite forms in close association with biotite, but does not replace it in those specimens examined.

Hornblende. Two varieties of hornblende have been

observed. One is green, moderately pleochroic and has an extinction angle of  $12^{\circ}$ . This mineral occurs in sample specimens 302 and 14. The first occurrence is in a volcanic conglomerate and the second in aphanitic latite. In both specimens andesine is unaltered although the hornblende is being replaced by carbonate. The other variety is brown, displays strong pleochroism and has an extinction angle of  $15^{\circ}$ . It occurs only in the crystal tuff of unit D where it also is partially replaced by carbonate (specimen 216).

Elsewhere relic phenocrysts of hornblende, recognized by remanent cleavages, are abundant. Montmorillonite or kaolinite rimmed by hematite in a distinct zonal pattern typically follow hornblende in a volume for volume replacement. Potassium feldspar, gypsum, calcite and quartz, also rimmed by hematite have also been observed as a replacement of hornblende. Examples of these types of alteration can be found in samples 82II, 145, 128 and 197I respectively. In intensely argillically altered rock, hornblende phenocryst outlines are preserved by hematite ghosts.

Potassium Feldspar. Clear sanidine phenocrysts, although rare, have been observed in several crystal tuff specimens (specimens 202, 216 and 82I). In addition, a few small perthites have been recognized (specimen 128). Elsewhere potassium feldspar, revealed by thin section staining and x-ray diffraction, occurs only in the micro-

crystalline groundmass of specimens.

A group of specimens, 29, 148, 6II, 13I, 155 and 188 display andesines which are mottled or rimmed by potassium feldspar. Although in general this potassium feldspar appears to be primary, in some instances it may be the result of exchange reactions with a hydrothermal fluid. Potassium feldspar is extremely resistant to alteration and persists even in intensely argillized regions.

Quartz. Quartz occurs both as monocrystalline clasts and polycrystalline aggregates in pyroclastic rocks. Quartz with rounded, blebby outlines is typical of crystal tuff. Polycrystalline quartz is common in agglomerate or conglomerate, as are arenaceous patches of quartz sand. Primary quartz is unaffected by hydrothermal alteration.

#### Secondary phases

Aragonite. Aragonite is the only phase precipitating from the Red Hill and Monroe springs. It forms knobby growths which line the spring channel.

Secondary Biotite. These deep red, blebby biotites are common in many propylitically altered rocks. They form in patches of hematite (specimen 1971) or inside partially altered primary biotite phenocrysts (specimen 158). In all cases the primary biotites, although altered, are not completely obliterated.

Biotite with Sapphiritic Rutile. These are primary biotites which have been partially altered to hematite,



kaolinite, and rutile. They are characterized by a cross hatching of rutile intergrowths. The occurrence of saginitic biotite appears to be limited to argillically altered rocks in the northwestern quadrant of the KGRA where it is closely associated with north trending fractures (figure 5). These specimens also exhibit considerable carbonate replacement.

Calcite and Dolomite. Calcite and dolomite are ubiquitous as replacement minerals. The two carbonates are frequently found together, but more generally one occurs to the exclusion of the other. There is, however, no special significance attached to the occurrence of dolomite versus calcite.

Plagioclase and hornblende are most readily replaced by carbonate, although biotite and alkali feldspar may also be attacked. In many specimens carbonate occurs as patches or veinlets cross-cutting rock fabrics. Hematite often rims such patches.

Carbonate is an abundant phase in both propylitic and argillically altered rock. However, its occurrence in advanced argillic zones, or zones containing sulfate minerals, is highly restricted. Nonetheless, outcrops which have sustained extensive carbonate replacement will frequently adjoin advanced argillic zones (locations 6, 100 and 197). Minor amounts of microcrystalline calcite may occasionally be found in rocks which contain jarosite and gypsum. In this association it is unusually thickly

mantled by hematite.

Throughout the area old fault planes are coated with calcite and fractured outcrops are filled with carbonate. The highest concentration of these carbonate veins is along the range front and adjacent to landslide areas. Calcite which is brightly banded with iron oxides can be found immediately south of the Red Hill tufa mound at the bottom of a large wash.

Chlorite. Chlorite is of rare occurrence, being of minor importance in all but a few specimens, 51, 13I and 300. In 13I it occurs as a fracture filling in biotite phenocrysts. This chlorite, which is characterized by radiating fibres, is probably not a direct replacement of biotite. Magnesium chlorite is assumed to predominate based upon the intensity of the 14 angstrom x-ray peak following heating of clay slides to 700°C.

Goethite. Goethite occurs in the tufa mound at Red Hill together with hematite and frothy calcite. The iron minerals form dense black veins through the calcite and stain the tufa a bright red. The occurrence of goethite requires that either the tufa was deposited at temperatures below 40°C (Berner, 1969) or that cool, iron rich solutions permeated the porous tufa at some time after its deposition causing primary hematite to be replaced by goethite.

Gypsum. Gypsum occurs in veins and as fracture fillings in all argillically altered areas. It is not unusual to find gypsum and calcite together as at location

140 where large euhedral calcite and selenite crystals are intergrown. The occurrence of gypsum as a replacement mineral, however, is limited to advanced argillic zones. In this environment it is invariably observed in association with kaolinite and jarosite, which it replaces. Gypsum most frequently appears as irregular patches or veinlets cross-cutting rock fabrics. However, it is also found replacing phenocrysts of plagioclase or hornblende (specimens 155 and 611). Patches of gypsum are typically rimmed by hematite.

Hematite. Opaque minerals in altered specimens were assumed to be hematite. Hematite in the form of disseminated blebs is common in most specimens. In addition, hematite accompanied by calcite, gypsum, kaolinite, montmorillonite or sericite replaces phenocrysts of biotite and hornblende in all but the freshest rock. Chlorite, jarosite and hematite are the only iron bearing alteration minerals.

The matrix of agglomerate southeast of Red Hill Spring is substantially replaced by hematite as is also the matrix of some of the conglomerate in unit A. Biotites with saginitic rutile are common in these rocks. The iron bearing solutions which infiltrated these permeable rocks are associated with the north trending fractures in this region.

Jarosite. Jarosite, the iron end member of the alunite solid solution series, is diagnostic for the advanced

argillic alteration regime (figure 5). Identified on the basis of x-ray diffraction analysis, jarosite is never visibly crystalline. In most specimens, gypsum contains a feathery, highly birefringent substance which is presumed to be jarosite. Jarosite and gypsum may have formed contemporaneously, however, gypsum is believed to be a replacement of jarosite in most cases. The possibility that jarosite is itself a replacement of potassium alunite is impossible to evaluate. The metastable association of jarosite with minor quantities of calcite is occasionally observed.

Kaolinite. Kaolinite is the hallmark of argillic alteration, and is without question the most common alteration mineral in the KGRA. Massive replacement kaolinite outcrops along fractures immediately to the east of Red Hill Spring. These deposits may be white or stained red and gray by iron oxides. The textures of these rocks have been nearly obliterated, with only hematite ghosts remaining. Intensely kaolinized rocks frequently contain sulfate minerals. Kaolinite occurs as a replacement of all primary phases.

Potassium mica. Sericite, while never occurring in significant quantities, is an ubiquitous phase in propylitic, argillic and advanced argillic zones. It occurs as a replacement mineral after all primary phases. Coarsely crystalline potassium mica, presumed muscovite, is less common but has been observed replacing biotite (specimen

18711). In specimen 1111, a white mica with an unusually low  $2V$  ( $5^\circ$ ), possibly paragonite, occurs as patches inside calcite and is an apparent replacement of alkali feldspar. Muscovite after feldspar was also observed in specimen 129.

Mixed Layer Clay. Two varieties of mixed layer clay were identified by x-ray diffraction. Both varieties have unglycolated (001) basal spacings of approximately 10.8 angstroms. One, designated mixed layer Clay II, swells when glycolated, resulting in a broad reflection between 11 and 17 angstroms. Upon heating to  $300^\circ\text{C}$  both clays collapse to a 9.8 angstrom basal spacing. On the basis of these data, the mixed layer clays are presumed to contain interlayered potassium mica and montmorillonite. Because these clays cannot be distinguished in thin section it is likely that much of the microcrystalline clay identified as sericite is in reality mixed layer clay.

Manganese Hydroxide. Dense, jet black fracture fillings at locations 197 and 143 are comprised in part of manganese hydroxides. At location 143, adjoining the Monroe tufa mound, the fracture fillings are predominately calcite. At 197, however, the fracture fillings are nearly pure  $\text{Mn}(\text{OH})_4$  with subordinate halite. These minerals are not replacement phases and apparently bear no relationship to the alteration of the host rock which is argillically altered in the first case and propylitically altered in the second. Several springs with high manganese concentrations are found in the Central Sevier River

Valley. One, the Joseph Hot Spring, is closely related chemically to the Monroe and Red Hill Springs (Young & Carpenter, 1965). The source of the manganese is open to speculation. Manganese minerals have also been reported at the Abraham Spring KGRA by Callaghan & Thomas (1938).

Montmorillonite. Montmorillonite is not present in great abundance. Nevertheless, its occurrence serves as an important diagnostic feature for the propylitic alteration zone. Its presence, although difficult to verify in thin section is confirmed by x-ray diffraction. Two varieties with (001) basal spacings of approximately 12.5 and 13.4 angstroms when air-dried were recognized. These varieties are considered to be sodium montmorillonite and calcium montmorillonite respectively. The bright green appearance of many propylitically altered outcrops suggests that the variety nontronite predominates. Sodium montmorillonite has a very limited occurrence being confined to the vicinity of the Monroe and Red Hill springs (specimens 142, 148, 144 and 184). It is undoubtedly the result of post formational cation exchange with calcium deficient sodium chloride solutions. Sodium montmorillonite, however, is not stable with respect to the present spring solutions.

Montmorillonite occurs, for the most part, in relatively fresh rocks or rock that has undergone calcite replacement and is common as a replacement mineral after biotite and hornblende. It is frequently accompanied by

hematite.

Massive replacement montmorillonite occurs only in the vicinity of location 138 where Dry Hollow porphyritic andesite has been replaced by calcium montmorillonite.

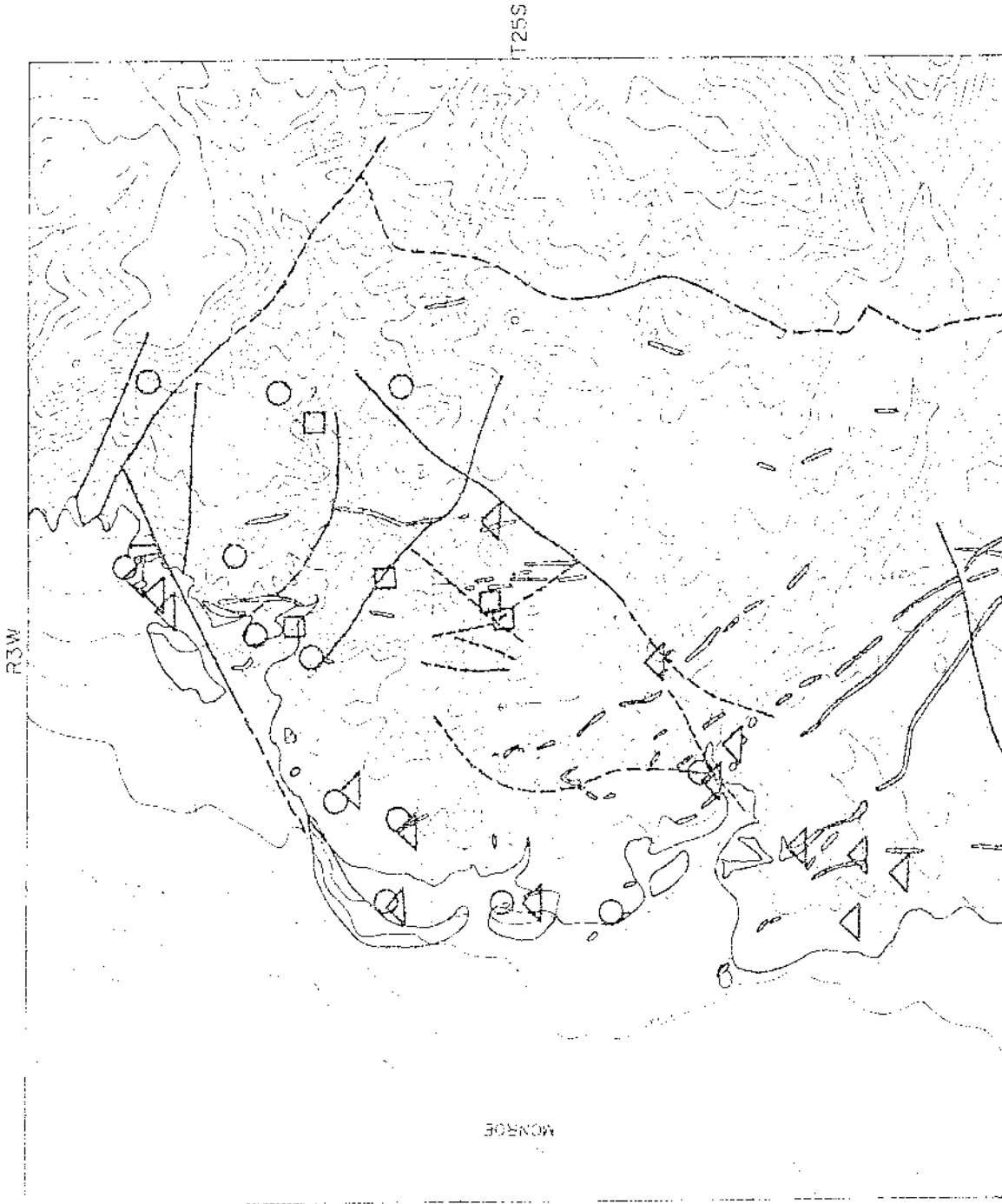
Quartz. Altered rocks of this area have been subjected to little if any silicification. Several large boulders of microcrystalline, milky white quartz outcrop at location 124. These boulders are enclosed by slightly dolomitized volcanic breccia and contain inclusions of mottled, dark red, hematite bearing quartz. No remnant feldspar has been detected by x-ray diffraction. It is, therefore, unlikely that this outcrop is silicified volcanic rock. A narrow fracture filling of this same milky quartz occurs at the intersection of two faults near Red Hill Spring (location 211). Microcrystalline quartz occurs as amygdules in porphyritic latite but is not common.

There is a higher incidence of polycrystalline quartz in altered rock suggesting that some of this may be secondary in origin. Secondary polycrystalline quartz is observed occupying a relic hornblende phenocryst in sample 197I. It therefore seems likely that quartz could be a product of the alteration of aluminosilicates by silica saturated solutions.

Native Sulfur. Tiny crystals between 10 and 50 micrometers in length of native sulfur are frequently found disseminated in the matrices of argillically altered rock.

Figure 5. Distribution of sulfate minerals, montmorillonite and biotite containing saganitic rutile.



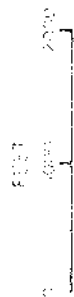


LEGEND

- ▲ EAST-WESTING
- WEST-EASTING
- WEST-NORTH-EASTING
- ▲ WEST-SOUTH-EASTING

- ▨ 100' contour
- ▩ 200' contour
- ▧ 300' contour
- ▦ 400' contour
- ▥ 500' contour
- ▤ 600' contour
- ▣ 700' contour
- ▢ 800' contour
- 900' contour
- 1000' contour
- ▟ 1100' contour
- ▞ 1200' contour
- ▝ 1300' contour
- ▜ 1400' contour
- ▛ 1500' contour
- ▚ 1600' contour
- ▙ 1700' contour
- ▘ 1800' contour
- ▗ 1900' contour
- ▖ 2000' contour
- ▕ 2100' contour
- ▔ 2200' contour
- ▓ 2300' contour
- ▒ 2400' contour
- ░ 2500' contour
- ▐ 2600' contour
- ▏ 2700' contour
- ▎ 2800' contour
- ▍ 2900' contour
- ▌ 3000' contour
- ▋ 3100' contour
- ▊ 3200' contour
- ▉ 3300' contour
- █ 3400' contour
- ▇ 3500' contour
- ▆ 3600' contour
- ▅ 3700' contour
- ▄ 3800' contour
- ▃ 3900' contour
- ▂ 4000' contour
- ▁ 4100' contour
- ▀ 4200' contour

- ANTI-CLING FAULT
- 10' FT
- 20' FT
- 30' FT
- 40' FT
- 50' FT
- 60' FT
- 70' FT
- 80' FT
- 90' FT
- 100' FT
- 110' FT
- 120' FT
- 130' FT
- 140' FT
- 150' FT
- 160' FT
- 170' FT
- 180' FT
- 190' FT
- 200' FT
- 210' FT
- 220' FT
- 230' FT
- 240' FT
- 250' FT
- 260' FT
- 270' FT
- 280' FT
- 290' FT
- 300' FT
- 310' FT
- 320' FT
- 330' FT
- 340' FT
- 350' FT
- 360' FT
- 370' FT
- 380' FT
- 390' FT
- 400' FT
- 410' FT
- 420' FT
- 430' FT
- 440' FT
- 450' FT
- 460' FT
- 470' FT
- 480' FT
- 490' FT
- 500' FT
- 510' FT
- 520' FT
- 530' FT
- 540' FT
- 550' FT
- 560' FT
- 570' FT
- 580' FT
- 590' FT
- 600' FT
- 610' FT
- 620' FT
- 630' FT
- 640' FT
- 650' FT
- 660' FT
- 670' FT
- 680' FT
- 690' FT
- 700' FT
- 710' FT
- 720' FT
- 730' FT
- 740' FT
- 750' FT
- 760' FT
- 770' FT
- 780' FT
- 790' FT
- 800' FT
- 810' FT
- 820' FT
- 830' FT
- 840' FT
- 850' FT
- 860' FT
- 870' FT
- 880' FT
- 890' FT
- 900' FT
- 910' FT
- 920' FT
- 930' FT
- 940' FT
- 950' FT
- 960' FT
- 970' FT
- 980' FT
- 990' FT
- 1000' FT



At sample location 1 euhedral acute bipyramidal sulfur crystals appear as inclusions in patches of calcite which are rimmed by hematite. Rounded, oblong crystals are clustered in calcite which has replaced hornblende in specimen 128. Hematite penetrates the calcite along relic amphibole cleavages.

#### Common Primary Textures

The rocks outcropping in the KGRA can be divided into two textural groups: volcanic flows and pyroclastic deposits. The flow rocks include porphyritic latite flows, doleritic latite dikes, and aphanitic latite dikes. The pyroclastic rocks include crystal tuffs, bedded tuffs and agglomerates. A third group of rocks, conglomerates and breccias, contain clasts from both groups. A remarkable degree of variety is displayed within each classification making correlation of outcrops very difficult. The problem is further complicated by the widespread hydrothermal alteration in this area.

#### Porphyritic latite

The most extensive outcrops of porphyritic latite flows occur in units C and E. These units can be differentiated on the basis of size of andesine phenocrysts and on the basis of magnetite content. Unit E is more coarsely porphyritic, and is characteristically a deep rust red.

The porphyritic latite of unit C contains large

andesine and hornblende phenocrysts. The largest of these are four and two millimeters in length respectively. Hornblende phenocrysts, however, are in general smaller than this, being 500 micrometers in length or smaller. The groundmass is a mosaic of tiny plagioclase laths, measuring approximately 50 micrometers in length. A few corroded biotites, less than one millimeter across, are sparsely distributed. All specimens display distinct flow structures. The appearance of porphyritic latite in thin section is more akin to the aphanitic than the doleritic latite found in the dikes.

#### Aphanitic Latite

Aphanitic dikes are characterized by andesine and hornblende phenocrysts in a microcrystalline groundmass containing potassium feldspar. The andesine occurs as fine laths, approximately 120 micrometers in length. Hornblende phenocrysts are scattered through the matrix. These phenocrysts attain lengths of one or two millimeters. Settling structures are usually marked. Vesicular outcrops are also common. This rock grades smoothly into the porphyritic latite of unit C.

#### Doleritic Latite

Doleritic dikes contain phenocrysts of andesine and frequently biotite. The andesine occurs as tabular phenocrysts, approximately one millimeter across. Plagioclase laths in the groundmass with maximum lengths of 500 micrometers are probably alkali feldspar. Settling

structures are frequently observed in these groundmass feldspars. Biotite phenocrysts, when present, are intermediate in size, averaging about 700 micrometers. Biotite occurs as both tabular crystals and in shafts. Monocrystalline quartz clasts occur sporadically and rarely exceed 200 micrometers. They may have been introduced via incorporation of country rock. In altered outcrops this rock may be indistinguishable from pyroclastic rock.

#### Crystal Tuff

Two distinct crystal tuffs occur. The first, in unit A, is characterized by andesine phenocrysts which are approximately two millimeters across, and narrow biotite shafts ranging in length from several micrometers to one millimeter. Hornblende phenocrysts average 500 micrometers in length. Quartz clasts are about the same size.

The second tuff, from unit D, has larger andesines which commonly exceed three millimeters in length. Tabular biotites, approximately two millimeters across and frequently with warped or broken cleavages, are abundant. Smaller biotite laths also occur. Deep red hornblende phenocrysts, also two millimeters in length, are thickly distributed. Large rounded clasts of monocrystalline quartz, one or two millimeters in diameter, also occur. Unlike the tuff of unit A, this rock contains many accidental rock fragments. The crystallinity of the

matrix varies, resulting in a patchy appearance when viewed in outcrop. These patches are presumed to have resulted from the incorporation of lapilli.

Both tuffs have a distinctly clastic texture, with many of the phenocrysts broken or fractured. Their matrices are composed of fine fragments in a microcrystalline groundmass.

#### Bedded Tuff

Bedded tuff occurs as thin interbeds in both units B and A. It is characterized by a fine clastic texture made up of remarkably well sorted fragments of plagioclase, biotite, quartz and magnetite. The sorting may be the result of air fall or, perhaps, alluvial action. The fragments are angular and uniformly 200 to 400 micrometers in diameter. The matrix is microcrystalline potassium feldspar. In outcrop this tuff has a distinct arenaceous appearance.

#### Agglomerate

Agglomerate is texturally similar to doleritic latite in that it contains an aphanitic matrix comprised of plagioclase laths, 100 micrometers in length or less. Flow structures, preserved in these laths, are often observed. The agglomeratic texture is distinctly non-uniform compared to the textures of the lava flows, however. Andesine, biotite, quartz and hornblende can vary dramatically in size, habit and distribution. Phenocrysts do not exceed one millimeter in most outcrops, however.

Quartz occurs both as monocrystalline clasts and polycrystalline aggregates. Agglomerates often contain irregular pebbles of volcanic flows and may grade into breccia.

#### Alteration Assemblages

The alteration assemblages observed in the KGRA bear a strong resemblance to alteration assemblages in the oxidized zones of many hydrothermally altered areas. A zonal pattern of alteration can be generalized for these areas which contains, in succession outward; 1) an alunite-quartz zone 2) an argillic zone, which may be subdivided into potassium mica-kaolinite and mixed layer potassium mica-montmorillonite subzones and 3) a propylitic zone, which may be subdivided into montmorillonite-vermiculite and chlorite subzones (Hemley, et.al., 1969). The alunite-quartz zone is generally highly siliceous and may contain dickite, pyrite or diaspore. In the Monroe KGRA only the argillic zone is well developed. However, jarosite, an iron alum isomorphous with alunite, does occur in association with kaolinite and sericite and is a common feature in the most intensely altered areas. Outcrops of rock which have been substantially altered to montmorillonite and chlorite are rare (locations 138 and 51). More commonly montmorillonite occurs as a minor mineral at the extremities of hydrothermally altered areas or in association with kaolinite and mixed layer clays in

argillically altered regions. Using the zonal model of Hemley as a guideline, the following zones are proposed for Monroe.

Advanced Argillic: contains kaolinite and jarosite

Argillic: contains kaolinite and mixed layer clay  
but does not contain montmorillonite

Propylitic: contains montmorillonite and mixed layer  
clay

Advanced Propylitic: contains montmorillonite or  
chlorite to the exclusion of  
kaolinite and mixed layer clay  
(rare)

Carbonate is frequently associated with argillic, propylitic and advanced propylitic assemblages. The peculiar hematite-kaolinite alteration associated with the north trending structures of the central part of the KGRA constitute a special case of argillic alteration.

An example of a low temperature hydrothermal area with important parallels to the Monroe KGRA is the Nevada Goldfield district. The Goldfield district is important for its quartz-gold vein mineralization. In the peripheral oxidized zone of this area, kaolinite, frequently massive, occurs with quartz, alunite and pyrite. Native sulfur and diaspore are minor accessory minerals. Potassium mica (sericite) occurs sparsely. Gypsum is widely distributed in veins and patches both above and below the water table. Calcite is abundant in the propylitically altered areas. Of particular interest is the association of coarsely crystalline alunite with microcrystalline calcite,

kaolinite and sericite in some altered rhyolites  
(Ransome, et.al., 1909).

The alteration relationships in the Monroe KGRA,  
therefore, are consistent with the peripheral oxidized  
zone of a low temperature, sulfide dominated hydrothermal  
system.



## MULTIVARIATE ANALYSIS OF ROCK ALTERATION

### Methods

Because of the nearly universal superposition of alteration assemblages, the subtle differences between these assemblages from outcrop to outcrop, and the feeble apparent correlations between the occurrence of most phases, multivariate analytical techniques were adopted to determine more objectively the basic structure of the data. Three basic approaches were utilized: principle component analysis (PCA), cluster analysis of the raw data, and cluster analysis of the data after it had been transformed into factor scores on the principle axes selected by PCA. Clustering was conducted in both the Q mode, that is clustering of samples, and in the R mode, that is clustering of components.

The data consisted of the compositions of each of 95 samples which were reported in percent total pattern intensity attributable to 15 recurrent phases: quartz, plagioclase, orthoclase, calcite, dolomite, hematite, jarosite, gypsum, apatite, biotite, kaolinite, montmorillonite, chlorite, and two mixed layer clays. Thirty of the samples for which clay fraction x-ray diffraction data were available were analyzed separately as well as with the remainder of the data. Because the data were

normalized and because they were not standardized across the variables, bias was unavoidably introduced into the analysis. The result of analyzing data presented in this fashion is to enhance the effect of the variance attributable to the most abundant phases and to generate spurious negative correlations between minor and major phases. Because of the nature of the data, however, standardization, that is insuring that each variable population has a mean of zero and a standard deviation of one, was not considered to be a meaningful operation. The distortion due to this phenomenon is not believed to have appreciably affected the analysis.

Clustering was based on the degree of association between components or samples as defined by correlation coefficients. In one trial, however, the data was scaled to a presence-absence format and a simple taxonomic distance coefficient was used. In all, twelve cluster analysis trials were made.

Where correlations between the abundances of minerals are recognized by PCA or cluster analysis, reaction relationships are presumed to prevail. Groups of positively correlated minerals define alteration regimes or zones. Negative correlations between groups reflect the zonal sequence of alteration.

#### Principle Component Analysis (R Mode)

In the initial data set, each specimen is defined in

terms of fifteen variables or minerals. These variables will, in general, display a complex set of variance-covariance relationships. PCA selects a set of factors which are linear combinations of the initial variables. These factors are the eigenvectors of the variance-covariance matrix for the data set. The factors, unlike the initial variables, are orthogonal or contain no covariance. Therefore, each of the factors represents an independent and fundamental parameter influencing alteration. By studying the linear combinations of variables contributing to each factor, the relationships among the phases may be determined.

The variance for the 30 x 15 array was 15. Ten mutually orthogonal factors were selected which together accounted for 94.2 percent of the total variance. The principle factor loadings (eigenvectors) for the transformations are reported in table 1. Reference to that table shows that the first factor, accounting for 25.7 percent of the total variance, heavily weights the contribution of plagioclase, quartz, kaolinite, montmorillonite, jarosite, apatite and biotite. Quartz, jarosite and kaolinite enter with negative contributions. This is a forceful statement of the close association of the latter minerals and their strong negative correlation with the primary phases plagioclase, biotite, and apatite, as well as montmorillonite. This is the anticipated result if a central argillized zone passes outward to a

Table 1. Principle axis factor loadings for the 30 x 15 data array.

## PRINCIPLE FACTORS

<u>VARIABLE</u>	<u>FI</u>	<u>FII</u>	<u>FIII</u>	<u>FIV</u>	<u>FV</u>	<u>FVI</u>	<u>FVII</u>	<u>FVIII</u>	<u>FIX</u>	<u>FX</u>
QUARTZ	-.809	-.119	.175	.340	.169	.177	-.105	-.103	.187	-.020
PLAGIOCLASE	.883	.042	.010	-.145	-.048	.315	.052	-.003	-.031	-.028
ORTHOCLASE	.218	.733	-.047	-.268	-.200	-.368	-.141	-.226	-.205	-.019
CALCITE	.096	-.551	-.190	-.347	-.459	-.144	.342	.342	-.005	.141
DOLOMITE	-.050	-.467	-.344	-.044	.614	-.279	.311	-.132	-.002	-.224
HEMATITE	.119	-.197	-.268	.718	-.274	.099	-.241	.223	-.295	-.248
JAROSITE	-.603	.404	.492	.006	-.178	-.001	.278	-.146	-.069	-.178
GYPSUM	-.389	.509	.156	.140	.091	.204	.509	.436	-.105	.023
APATITE	.590	.018	.543	.039	.285	-.228	.011	.226	.206	-.168
BIOTITE	.557	-.059	.493	.246	.007	-.468	-.126	.219	-.019	.004
KAOLINITE	-.746	-.064	.068	.024	.123	-.280	-.303	.196	-.004	.379
MONTMORILLONITE	.633	.125	.016	.462	-.155	.165	.174	-.188	.348	.268
CHLORITE	.237	-.255	.463	-.343	.332	.499	-.234	.075	-.252	.092
MIXED LAYER CLAY I	-.025	.549	-.446	-.266	.112	.133	-.298	.385	.329	-.179
MIXED LAYER CLAY II	-.393	-.435	.360	-.266	-.506	.054	-.135	-.035	.229	-.259
Percent Variance	25.7	14.1	10.7	9.33	8.49	7.08	6.23	5.24	3.79	3.44

weakly propylitized zone. Factor one may be visualized as an index of pH or reaction progress. The groups obtained by cluster analysis are, for the most part, predicted on this factor.

Factor two is characterized by positive contributions from orthoclase, mixed layer clay I and gypsum, and by a negative contribution from calcite. It contains 14.1 percent of the total variance. It is apparent that the occurrence of calcite and gypsum is not linked to the degree of overall reaction progress, but is influenced by some independent property, presumably the  $PCO_2$  or  $PH_2S$  of the system. In addition, orthoclase and mixed layer clay I, both potassium phases, appear to be highly correlated and to be disfavored in the  $CO_2$  regime.

The third factor, accounting for 10.7 percent of the variance, appears to be a measure of the alteration of biotite and apatite, both highly resistant minerals. The apparent degeneracy of this factor with respect to factor one is not understood.

Factor four, with 9.3 percent of the variance is dominated by hematite. This factor, apparently an index of total iron molality or Eh, serves to distinguish the iron rich argillic alteration, associated with the north trending fractures, from the sulfate argillic alteration associated with northeast trending fractures and faults.

Factor five heavily weights the contribution of dolomite, mixed layer clay II and calcite. This factor

could be interpreted as an indicator of the concentrations of  $\text{Ca}^{+2}$  and  $\text{Mg}^{+2}$ . It accounts for 8.5 percent of the total variance.

Factor six contains 7.1 percent of the variance. It reflects the reaction relationship of chlorite and biotite. This is the last factor from which information can readily be gleaned. The remaining factors together account for less than 19 percent of the variance.

In summary, PCA of the 30 x 15 matrix reveals that a particular sample can be virtually defined by 10 orthogonal vectors as opposed to the 15 variables in the original data set. Therefore, the original set of variables must contain a substantial degree of covariance. This is useful since it means that reaction relationships among the phases have not been totally obscured. Furthermore, positive correlations are inferred for the following mineral pairs: jarosite-kaolinite, quartz-kaolinite, montmorillonite-plagioclase, montmorillonite-biotite, apatite-biotite, gypsum-mixed layer clay I, gypsum-orthoclase, dolomite-calcite, and mixed layer clay II-calcite. Negative correlations are inferred for the following mineral pairs: chlorite-biotite, calcite-orthoclase, calcite-gypsum, kaolinite-plagioclase, kaolinite-montmorillonite, and kaolinite-biotite.

Groups of phases defining alteration regimes are:

- i) plagioclase, biotite, apatite and montmorillonite,
- ii) kaolinite, jarosite and quartz, iii) orthoclase, mixed

layer clay I and gypsum and iv) calcite, dolomite, and mixed layer clay II. Negative correlations between these groups suggest that group ii is an alteration product of group i and that group iv is an alteration product of group iii.

The variance of the 95 x 15 array was also 15. Ten factors were selected which cumulatively accounted for 88.3 percent of the total variance. The first factor contains 19.6 percent of the total. The principle factor loadings are reported in table 2. The similarity of the two data sets lends confidence to the interpretation based on the PCA of the more detailed 30 x 15 array. However, several important associations were emphasized in this analysis which were not apparent in the previous run. In particular, a positive correlation between montmorillonite and calcite is inferred from the loadings for factor five.

The clarity of the PCA for these and similar data sets would be greatly improved if a factor rotation routine such as the Kaiser verimax scheme were adopted. This procedure optimizes the factor loadings to values approaching one or zero by fixed rotation of the principle vectors. However, due to limited time, funds and expertise this was not attempted. As it has been utilized in this study, PCA fosters an intuitive feel for the structure of the data and provides useful guidelines for

Table 2. Principle axis factor loadings for the 95 x 15 data array.

PRINCIPLE FACTORS

<u>VARIABLE</u>	<u>FI</u>	<u>FII</u>	<u>FIII</u>	<u>FIV</u>	<u>PV</u>	<u>FVI</u>	<u>FVII</u>	<u>FVIII</u>	<u>FIX</u>	<u>FX</u>
QUARTZ	.727	-.454	.080	.031	-.325	-.029	.015	-.105	.090	-.086
PLAGIOCLASE	-.783	.175	-.024	-.223	-.120	-.398	-.146	-.155	-.016	.128
ORTHOCLASE	-.134	.713	-.014	-.099	.076	.080	.547	.029	.030	-.155
CALCITE	-.096	-.340	-.150	-.073	.552	-.141	.176	.645	-.246	-.082
DOLOMITE	.007	-.164	-.077	.800	.007	-.079	-.075	-.166	-.409	.137
HEMATITE	-.192	-.549	-.196	-.319	-.336	.138	-.188	.227	.263	.045
JAROSITE	.687	.355	.010	-.365	.009	-.069	-.165	-.061	-.253	.083
GYPSUM	.524	.408	-.125	-.182	-.184	-.065	-.452	.293	-.261	.027
APATITE	-.170	.134	.758	.071	-.060	-.034	-.113	.260	-.071	.278
BIOTITE	-.146	-.147	.488	-.075	-.357	.520	.241	.143	-.244	.103
KAOLINITE	.815	.030	.116	.144	.070	.077	.145	.041	.104	-.193
MONTMORILLONITE	-.130	.211	.011	.061	.518	.674	-.401	-.098	.194	.022
CHLORITE	.011	.002	.699	.104	.168	-.362	-.205	.031	.376	-.325
MIXED LAYER CLAY I	.184	.357	-.228	.467	-.200	-.075	.032	.396	.476	.300
MIXED LAYER CLAY II	.475	-.196	.146	-.280	.411	-.152	.257	-.211	.146	.509
Percent Variance	19.6	11.6	0.85	8.77	8.13	7.41	6.58	6.15	5.84	4.43



further analysis.

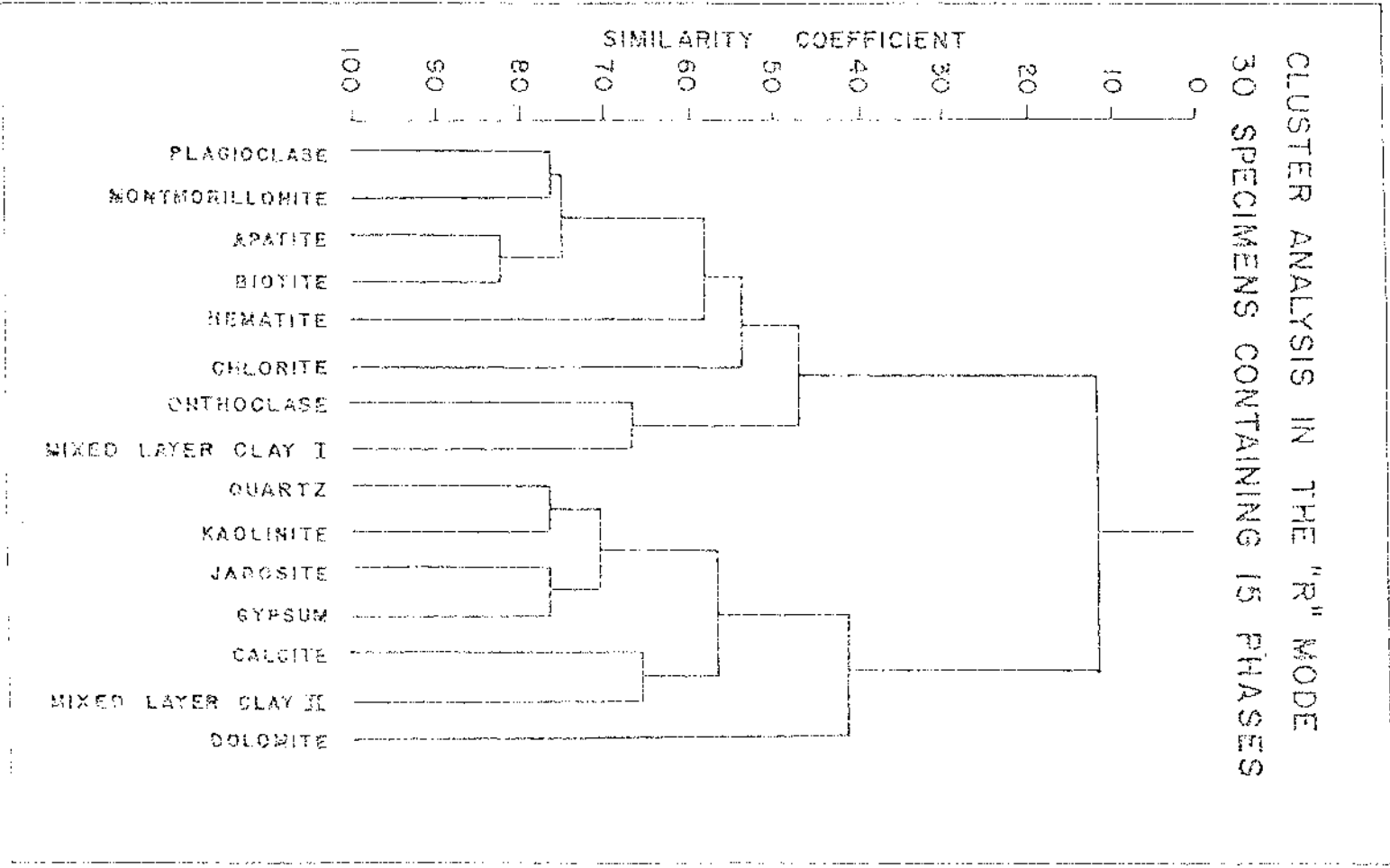
### R Mode Cluster Analysis

R mode cluster analysis is a technique in which the initial data matrix is transposed and correlation coefficients are calculated between the phases. Pairs of phases with mutually high correlation coefficients are linked at high degrees of similarity. In succeeding steps new phases are added to groups or existing groups are linked as increasingly lower correlations are accepted into the cluster. Groups of phases which are clustered with a high degree of similarity have strong positive correlations and may be regarded as defining alteration regimes.

R mode cluster analysis was employed in order that the relationships prevailing among the phases might be displayed in a more straightforward and graphic fashion. Cluster analysis of raw data for both arrays was carried out. In addition, cluster analysis was conducted on the 30 x 15 array after the data had been transformed into factor scores following PCA. Factors were weighted according to their percent variance. The results of all three trials were similar (figure 6).

Highly correlated mineral pairs are plagioclase-actinolite, orthoclase-mixed layer clay I, quartz-epidote, jarosite-gypsum, and mixed layer clay II-silicate. More distantly clustered groups of phases are

Figure 6. R mode cluster of raw 30 x 15 array.



plagioclase-montmorillonite-chlorite, and mixed layer clay II-calcite-jarosite-gypsum-quartz-kaolinite. These relationships compare very favorably with the deductions which were based on PCA. Unfortunately, cluster analysis is very ambiguous with respect to negatively correlated phases. In presenting an overall understanding of the dynamics of alteration reactions PCA may be more effective.

For one trial the 95 x 15 array was scaled to a presence-absence format and clustered using a simple taxonomic distance function. This run did not result in meaningful clustering.

As an aid to interpreting the results of PCA and cluster analysis a graphic approach was adopted. The percent pattern intensities of montmorillonite, chlorite, mixed layer clay I, mixed layer clay II and jarosite were plotted against the index phases plagioclase, kaolinite and carbonate for the 30 x 15 array. The plots are presented in figures 7 and 8. Dotted lines have been added in order to emphasize the limiting correlative relationships. They have no statistical significance.

Mixed layer clay I does not occur with sufficient frequency to draw any conclusions. Montmorillonite is stable at high percentages of plagioclase and when present is roughly proportional to plagioclase. It is inversely proportional to kaolinite, never being observed in specimens containing more than 12 percent kaolinite.

Figure 7. Abundances, reported in percent pattern intensity, of four alteration minerals versus plagioclase and kaolinite.

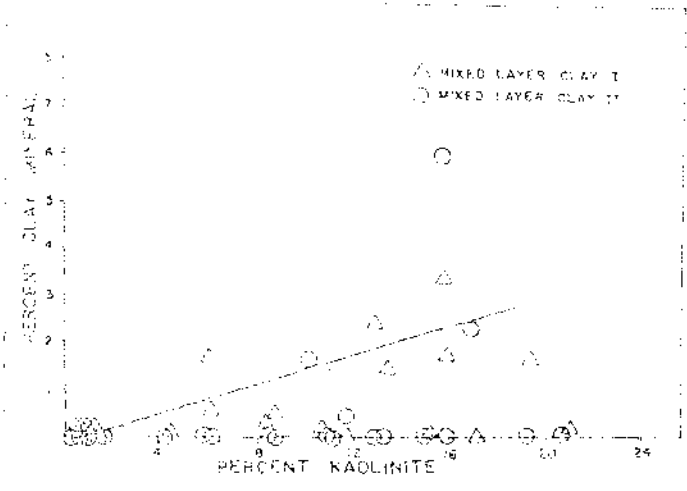
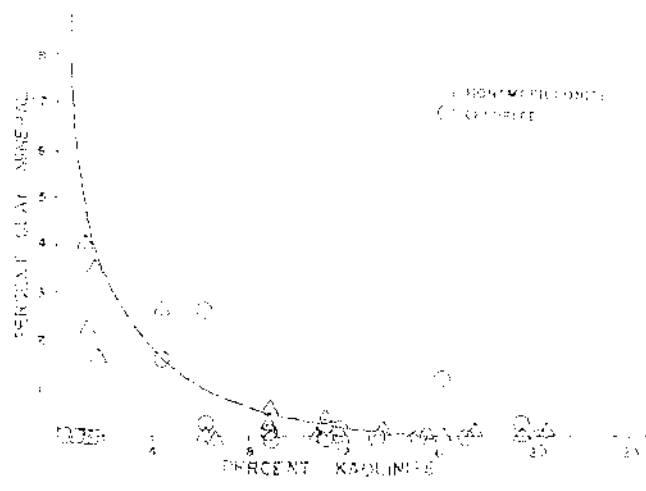
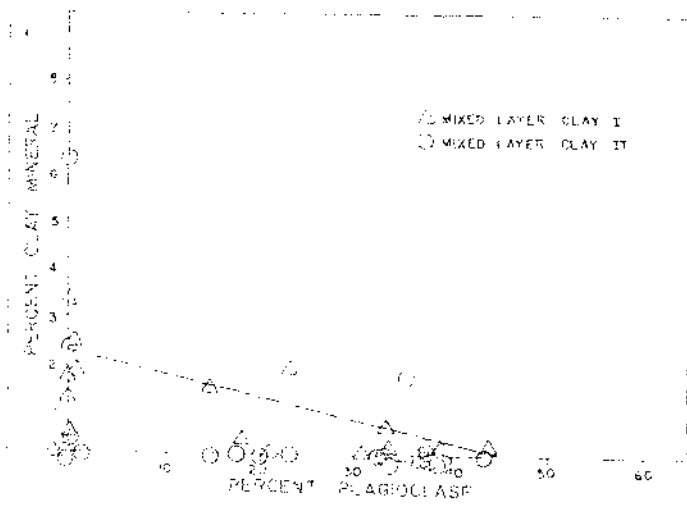
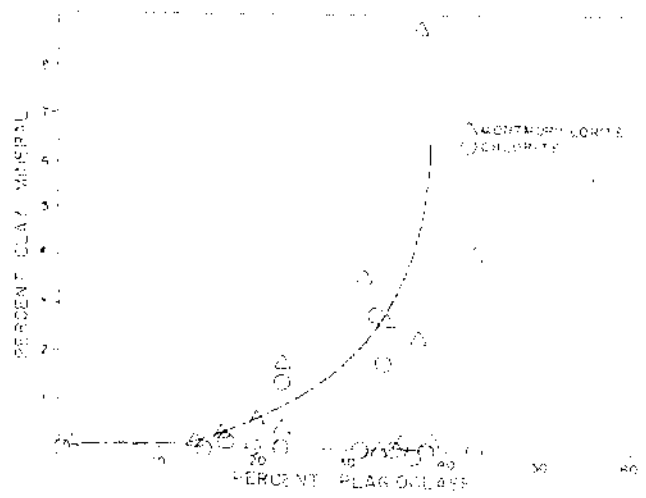
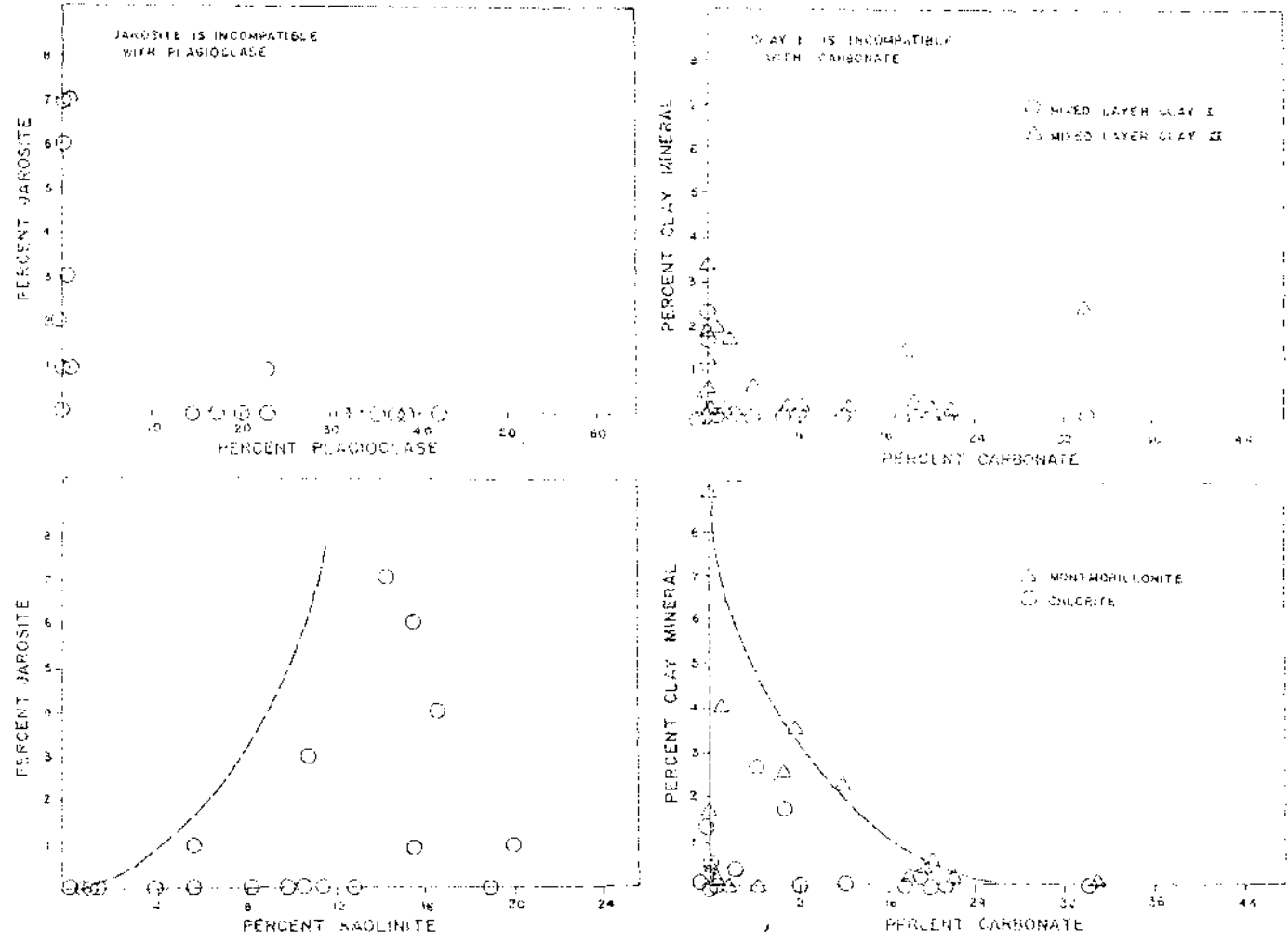


Figure 8. Abundances, reported in percent pattern intensity, of five alteration minerals versus plagioclase, kaolinite, and carbonate.





specimens, cluster analysis was again employed. Cluster analysis permits the extension of alteration zone definitions to specimens which do not contain the diagnostic minerals montmorillonite and jarosite and to specimens which contain metastable mineral associations. Q mode cluster analysis is similar to R mode cluster analysis except that correlation coefficients are calculated among the specimens. Specimens contained in the same cluster are petrologically similar and may be regarded as belonging to the same alteration zone. Three approaches were taken: 1) Raw arrays were clustered. 2) Arrays were clustered after the data had been transformed into factor scores and the factors weighted according to their percent variance. 3) Arrays were clustered after the data had been transformed into factor scores and the first factor deleted.

By deleting the factor containing the highest percentage of the total, it was intended to compensate for the bias introduced by normalizing the data. Because most of the variance is attributable to the most abundant phases, removing a high variance factor should enhance the contribution of the minor minerals in the cluster analysis.

Deletion of the first factor resulted in poorly clustered or nonclustered trials. Other trials produced a variety of related clustering patterns which were, for the most part, predicted on variations in kaolinite,

plagioclase and carbonate. Those trials for which the data had been transformed into factor scores were most sensitive to the presence of carbonate. When evaluated on the basis of PCA and R mode cluster analysis, Q mode cluster analysis of raw unscaled data produced the most rational groupings of specimens. The results are presented in figure 9. A histogram showing the distribution of phases among the clusters is presented in figure 10.

Four clusters were obtained. Cluster I contains specimens which share in common a low percentage of plagioclase, a high percentage of kaolinite and are more apt to contain jarosite, gypsum or mixed layer clays. Cluster III specimens have the highest percentages of plagioclase and low percentages of kaolinite. This group is more apt to contain montmorillonite. Cluster II specimens are intermediate in their characteristics between clusters I and III and are more apt to contain high percentages of carbonate. Cluster IV contains specimens with high percentages of plagioclase but otherwise is poorly defined. This cluster was discarded.

In general cluster I can be identified with acid sulfate alteration, cluster II with carbonate argillic alteration, and cluster III with a weakly propylitic alteration. When plotted on the base map in figure 11 the specimens of cluster I and II are observed to follow the major northeast trending structures. The specimens of cluster I, however, occupy the most intensely altered

Figure 9. Q mode cluster analysis of raw 95 x 15 array.

CLUSTER ANALYSIS IN THE "Q" MODE  
95 SPECIMENS CONTAINING 20 PHASES

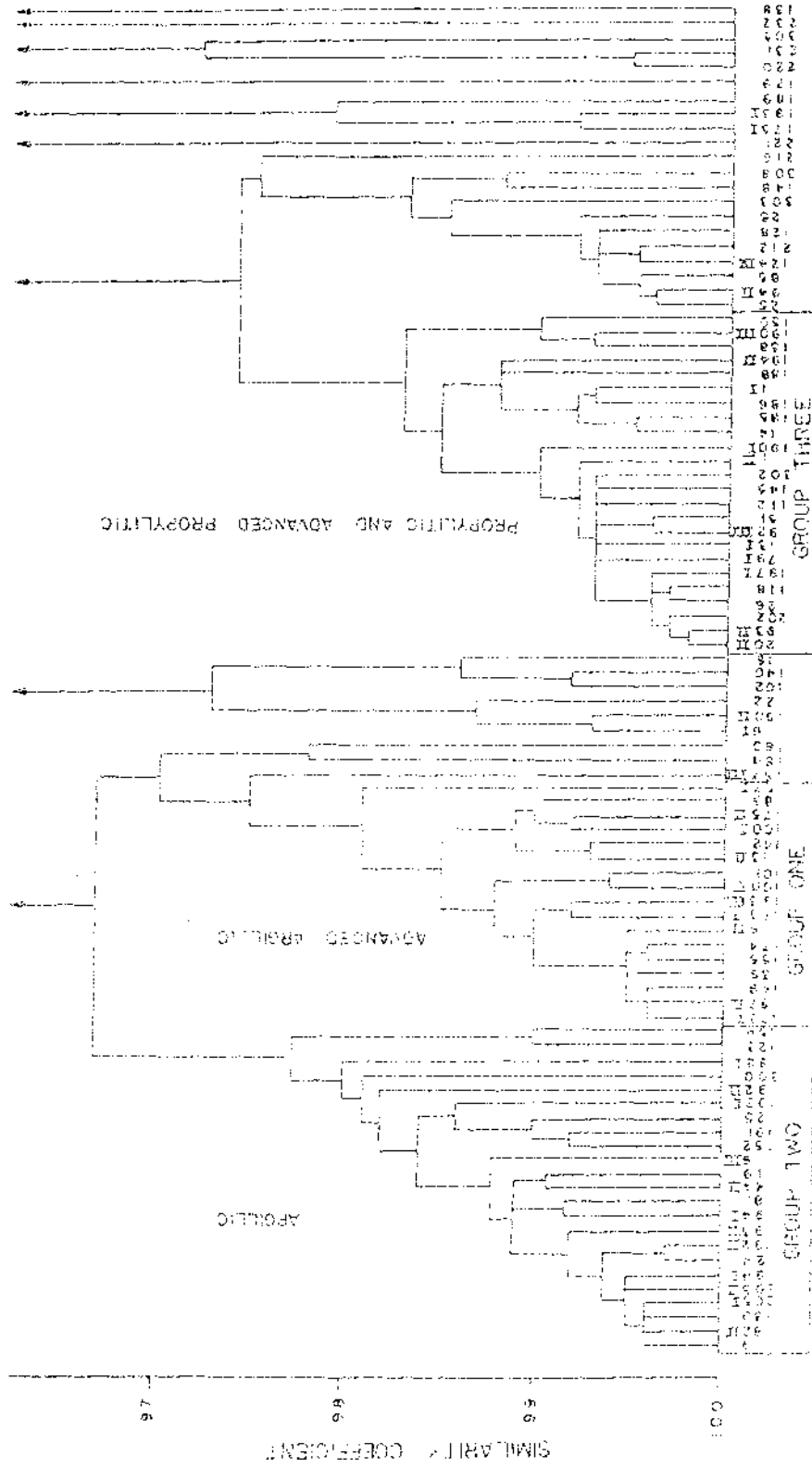


Figure 10. Histograms showing the distribution of phases among the three clusters chosen from cluster analysis of raw 95 x 15 array. Values of "volume percent" are percent pattern intensities.

# DISTRIBUTION OF PHASES IN CLUSTER GROUPS

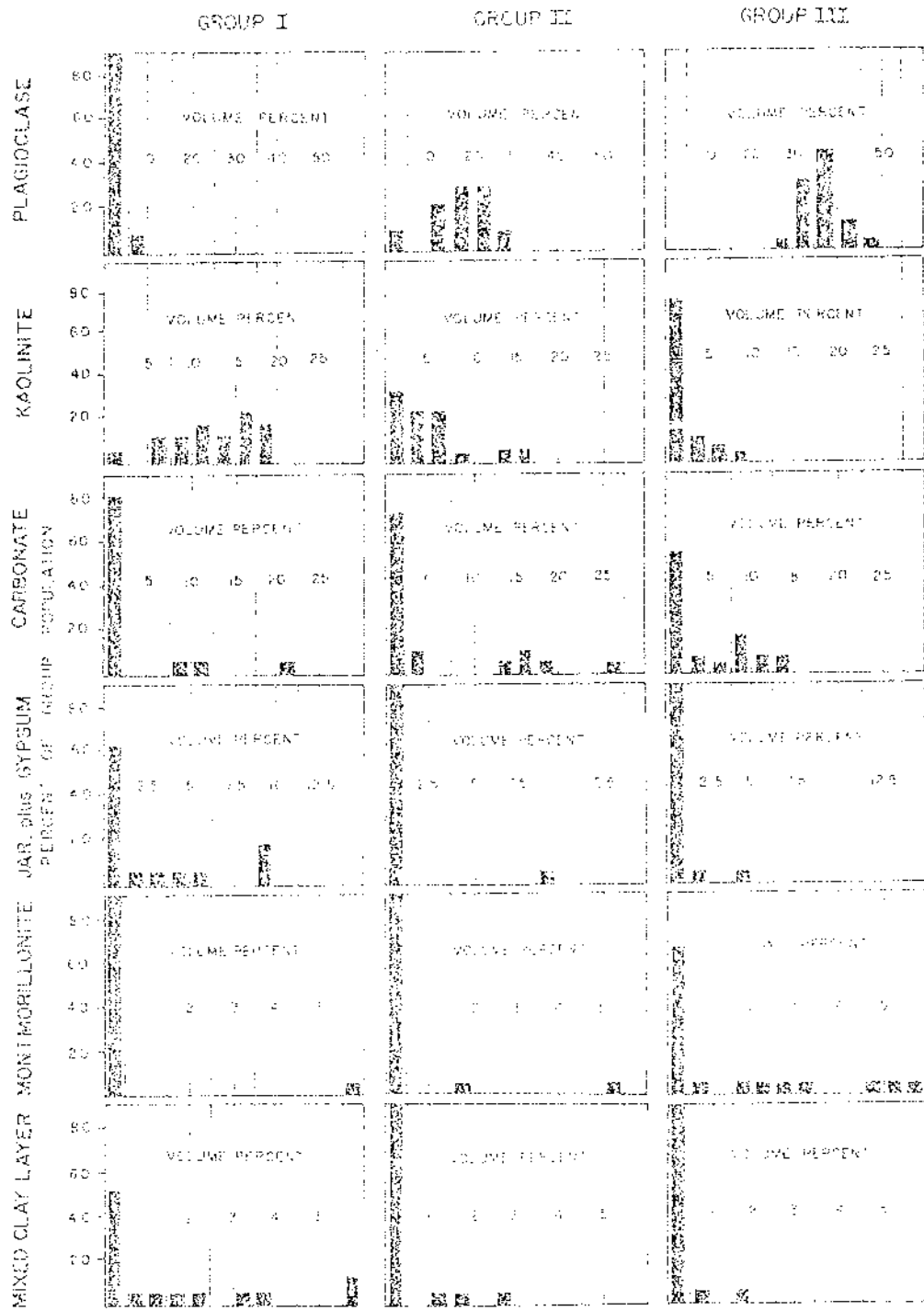
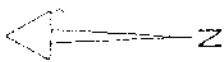
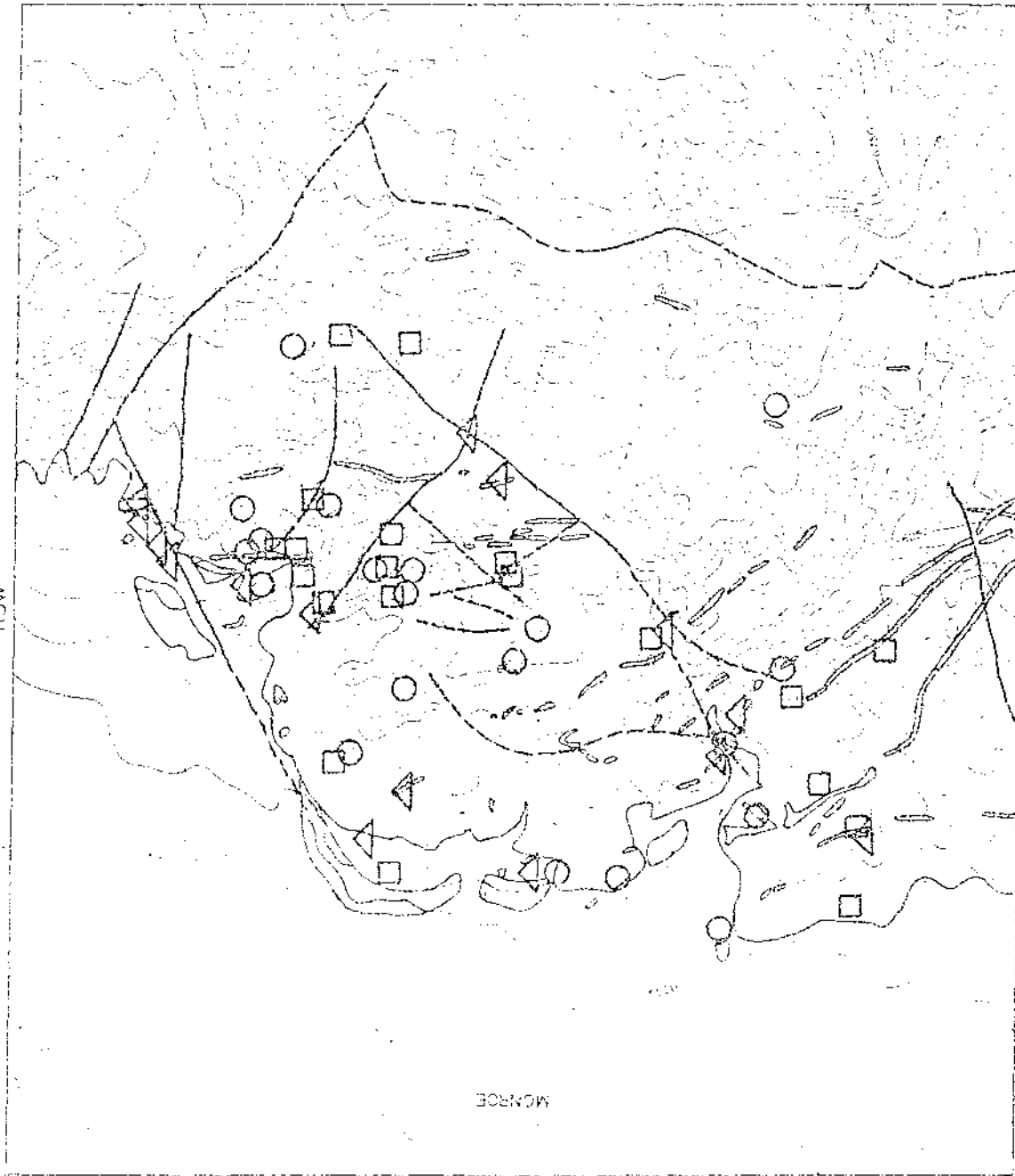


Figure 11. Areal distribution of three clusters chosen from cluster analysis of raw 95 x 15 array.

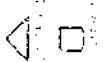
T25S

R3W

MORROE



LEGEND



WATER



WATER



WATER



WATER

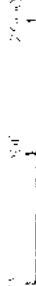


WATER

WATER

WATER

100'





areas. A boundary appears to exist near location 124 (figure 4), north of which cluster I does not penetrate. Cluster II specimens are heavily concentrated along the north trending structures as well. This suggests that some of the specimens in cluster II may represent a separate genetic group. Cluster III is more diffusely distributed. These specimens frequently occupy locations peripheral to the most intensely altered rock. Cluster III specimens are also typical of leached outcrops. A distinct zonal arrangement, therefore, is apparent which passes outward from an acid argillic zone to a carbonate argillic zone and then to a weak propylitic zone.

## SPRING GEOCHEMISTRY

### Methods

The water from the Red Hill and Monroe Springs was sampled and analyzed following the procedures outlined by Presser and Barnes (1974). The concentrations of the following ions were determined.

$\text{Sr}^{+2}$ ,  $\text{Ca}^{+2}$  and  $\text{Mg}^{+2}$ : A one liter sample of spring water was filtered through a .1 micrometer filter under compressed nitrogen and then acidified to pH 2 with HCl. The ion concentrations were determined using a Perkin-Elmer 303 atomic absorption spectrometer.

$\text{Na}^+$ : A one liter sample of spring water was filtered through a .1 micrometer filter under compressed nitrogen. The ion concentrations were determined by atomic absorption spectrometry. The results were checked against the activities of sodium measured directly using an Orion select ion probe and pH meter.

$\text{Cl}^-$ : A one liter sample of spring water was filtered through a .1 micrometer filter under compressed nitrogen. The ion concentration was determined via a Mohr titration. The results were checked against the activities of chloride measured by select ion probe.

$\text{SO}_4^{-2}$ : A one liter sample of spring water was filtered

through a .1 micrometer filter under compressed nitrogen and treated with chloroform. The ion concentrations were determined using an indirect atomic absorption technique.

$S^{-2}$ : A 100 milliliter sample of spring water was collected and the sulfide fixed by addition of zinc acetate and sodium hydroxide. Specimens were titrated the same day using an iodine-thiosulfate backtitration technique. Results of the titration were checked against the sulfide activities obtained by select ion probe.

$HCO_3^-$ : An untreated sample was titrated with standard HCl to a methyl orange endpoint.

$H_4SiO_4$ : A one milliliter sample was diluted 1:10 and stored in a plastic container. Silica concentrations were measured the next day by atomic absorption.

pH: Hydrogen ion activity was measured using a glass electrode and pH meter standardized to the temperature of the spring.

Sulfide was below the detectable limit,  $10^{-6}$  moial in both springs. The measured concentration of the remaining species are reported in table 3.

The composition of spring gases was also determined. For this determination a gas sample was obtained by displacement of spring water from a two liter glass bottle. The sealed bottle was then connected to a gas train and the contained gases forced through a series of solution traps by compressed nitrogen. Oxygen was determined using a modified Winkler titration and hydrogen sulfide using the

Table 3. Warm spring waters in the Monroe area.

	MONROE	RED HILL	JOSEPH <sup>2</sup>
$m_{Ca^{+2}}$	.0074	.0069	.0070
$m_{Na^{+}}$	.026	.025	.063
$m_{K^{+}}$	.0014	.0013	.0017
$m_{Mg^{+2}}$	.0015	.0015	.0015
$m_{Cl^{-}}$	.019	.020	.049
$m_{HCO_3^{-}}$	.0076	.0070	.0070
$m_{SO_4^{-2}}$	.010	.011	.013
$m_{H_4SiO_4^0}$	.00032	.00021	.00089
pH	6.1	6.6	6.6
Temp( <sup>o</sup> C)	59	77	65

2 - analysis by U.S.G.S. (Young and Carpenter, 1965)

same method employed for the dissolved sulfide determination. Carbon dioxide was trapped in standard barium hydroxide solution, which was then back titrated with standard HCl. Only carbon dioxide was detected in each sample.

#### Calculation of Ion Activities

High temperature dissociation constants and equilibrium constants were taken from Helgeson (1969), tables 4, 11 and 12. Dissociation constants at 25° centigrade for certain aqueous complexes were taken from Garrels & Christ (1965). Activity coefficients were calculated using the Debye Huckel relation and deviation function as tabulated in Helgeson (1969), table 2. The assumption was made in these calculations that Ba equals 1.5 (Nraigu, 1971).

In calculating the activities of the major ions in the Red Hill Spring water, the following complexes were considered;  $\text{CaSO}_4^0$ ,  $\text{CaCO}_3^0$ ,  $\text{CaHCO}_3^-$ ,  $\text{NaHCO}_3^0$ , and  $\text{NaSO}_4^-$ . The molality of  $\text{Mg}^{+2}$  and  $\text{K}^+$  were low enough such that complexes containing these ions need not be considered. Since high temperature thermodynamic data on  $\text{CaHCO}_3^+$ ,  $\text{NaHCO}_3^0$  and  $\text{NaSO}_4^-$  was not available, the values of dissociation constants at 25° centigrade were used in calculations of ion activities below 75° centigrade. At higher temperatures the activities of  $\text{CaHCO}_3^+$  and  $\text{NaHCO}_3$  were not considered and the dissociation constant of  $\text{KSO}_4^-$  was assumed to be sufficiently similar to  $\text{NaSO}_4^-$  to be used in its place. The activity of neutral complexes was assumed to be unity. In

addition the activity of  $\text{Na}^+$  was treated as a constant, as was also pH.

Given these assumptions the activities of the major ions were calculated for a temperature of  $75^\circ$  centigrade, a pH of 6.6 and a molality of  $\text{Na}^+$  of .0255. The results of these calculations are in table 4.

It is apparent that any errors introduced by assumptions made about the complexes  $\text{CaHCO}_3^+$  and  $\text{NaHCO}_3^0$  will be small. The spring water is saturated with respect to gypsum and quartz at the temperature of the flowing spring and slightly oversaturated with respect to calcite. The calculated  $f\text{CO}_2$  is consistent with saturation with respect to  $\text{CO}_2(\text{g})$  at a depth of approximately 25 feet, assuming a hydrostatic pressure gradient of .028 atmosphere per foot. Therefore a slight oversaturation in calcite is apt to prevail at the surface as  $\text{CO}_2$  gas separates from the solution in the last few feet of ascent.

The activities of the major ions in the Joseph Hot Spring water reported in table 5 shows that it is chemically very similar to that of the Red Hill Hot Spring and, like that spring, saturated with respect to calcite and gypsum at the spring temperature.

#### Origin of the Monroe Spring Water

In considering the chemistry of the Monroe Spring system, the chemical composition of the Red Hill Spring has been used to the exclusion of the Monroe Spring. This

Table 4. Activities of aqueous species in the Red Hill Spring.

Temperature 75°C

pH 6.6

<u>Species</u>	<u>Activity</u>
$\text{Ca}^{+2}$	.0019
$\text{SO}_4^{-2}$	.0035
$\text{Na}^+$	.021
$\text{Cl}^-$	.021
$\text{HCO}_3^-$	.0030
$\text{CO}_3^{-2}$	$8.4 \times 10^{-7}$
$\text{K}^+$	.001
$\text{Mg}^{+2}$	.0006
$\text{CaSO}_4^{\circ}$	.0026
$\text{NaSO}_4^-$	.00039
$\text{CaHCO}_3^+$	.00010
$\text{NaHCO}_3^{\circ}$	.000035
$\text{H}_4\text{SiO}_4^{\circ}$	.00021
$f\text{CO}_2 = .12$	
$I = .03$	
$\log(a_{\text{Ca}^{+2}} \times a_{\text{SO}_4^{-2}}) = -5.2$	$\log K_{\text{gypsum}} = -5.3$
$\log(a_{\text{Ca}^{+2}} \times a_{\text{CO}_3^{-2}}) = -8.8$	$\log K_{\text{calcite}} = -9.0$

Table 5. Activities of aqueous species in the Joseph Hot Springs.

Temperature 65°

pH 6.6

<u>Species</u>	<u>Activity</u>
Ca <sup>+2</sup>	.0020
SO <sub>4</sub> <sup>-2</sup>	.0032
Na <sup>+</sup>	.052
Cl <sup>-</sup>	.029
HCO <sub>3</sub> <sup>-</sup>	.0030
CO <sub>3</sub> <sup>-2</sup>	8.4 x 10 <sup>-7</sup>
K <sup>+</sup>	.0014
Mg <sup>+2</sup>	.00066
H <sub>4</sub> SiO <sub>4</sub> <sup>0</sup>	.00088
fCO <sub>2</sub> = .10	
I = .05	
log(a <sub>Ca</sub> <sup>+2</sup> x a <sub>SO<sub>4</sub><sup>-2</sup>) = -5.2</sub>	log K <sub>gypsum</sub> = -5.2
log(a <sub>Ca</sub> <sup>+2</sup> x a <sub>CO<sub>3</sub><sup>-2</sup>) = -8.8</sub>	log K <sub>calcite</sub> = -8.8



is because the chemistry of the two springs are similar and because Red Hill Spring has the higher temperature and greater flow rate of the two.

The water contained in the hot springs of this area has equilibrated with calcium carbonate before outcropping at the surface. The most likely site for this equilibration is the limy beds of the Carmel formation which directly underlies the Bullion Canyon volcanics.

It is considered unlikely that the spring waters represent fluids which have equilibrated at high temperatures with sedimentary carbonate rock and then risen without further alteration save adiabatic cooling and separation of carbon dioxide gas. The hypothetical compositions of fluids saturated with respect to gypsum and calcite at elevated temperatures were calculated. In order to maintain ionic strengths similar to those at Red Hill without increasing the molality of NaCl, lower pH's and higher carbon dioxide fugacities are required. Due to the elevated fugacities of carbon dioxide in these fluids, separation of carbon dioxide would begin at considerable depths, nearly 1400 feet at 150°C if a hydrostatic pressure gradient is assumed. This would cause the solutions to be significantly undersaturated with respect to calcite at the surface. A high temperature reservoir, therefore, can be the immediate source of the spring water only if complete re-equilibration with calcite at a lower temperature and pH occurs.

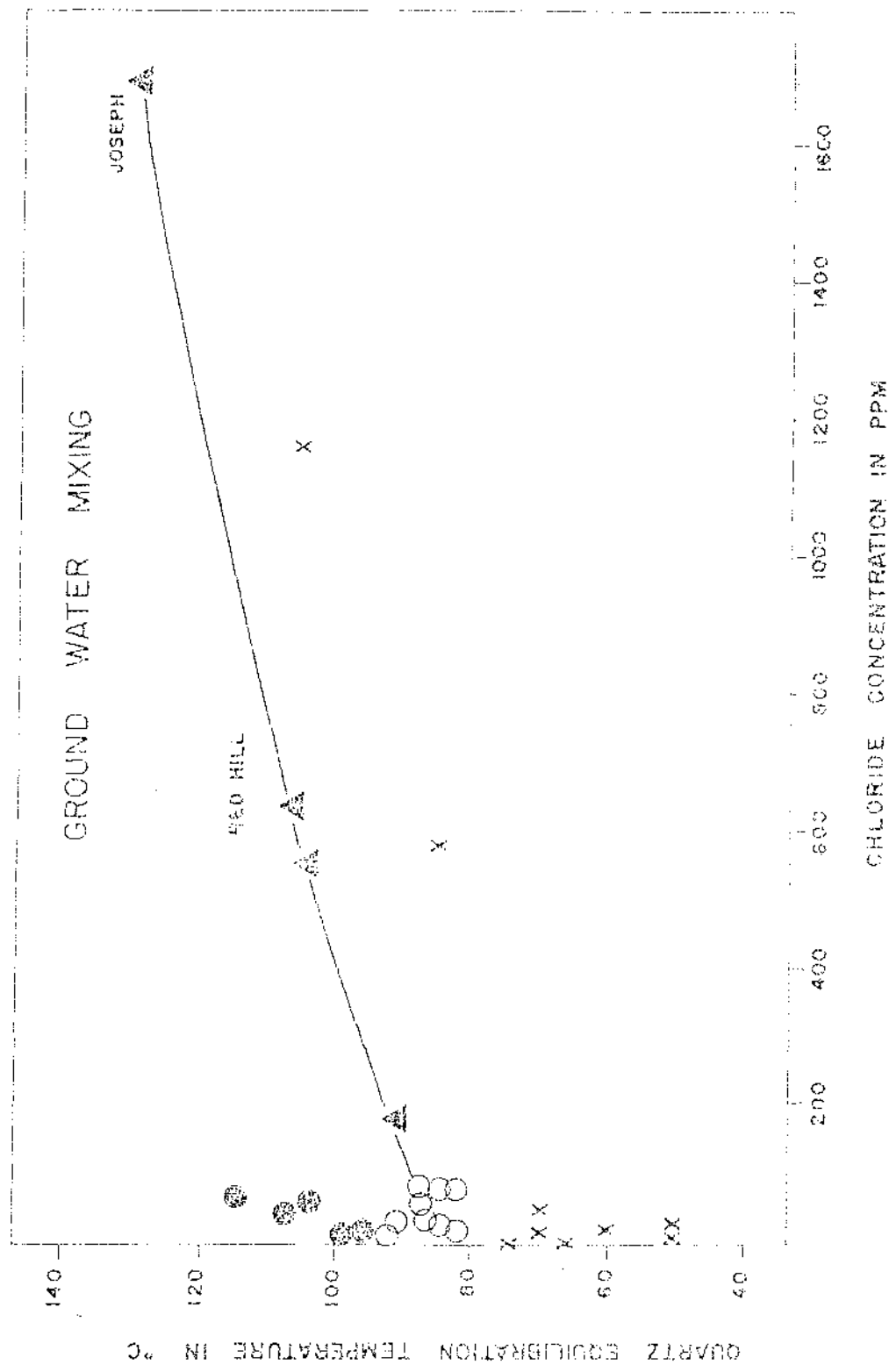
Mixing of high and low temperature solutions is considered a plausible origin of the spring waters. Unfortunately, the warm spring mixing formulae proposed by Fournier and Truesdall (1974) are not applicable to this system because the flowing spring is saturated with respect to quartz. Provided there is mixing of solutions in the system, it is apparent that the mixtures have re-equilibrated with silica at the temperature of mixing. The temperature of the Red Hill Spring, 75° centigrade, probably represents the temperature of mixing for that particular solution.

If mixing does prevail, mixing temperatures, taken as the quartz saturation temperatures, should be proportional to the degree to which a hot source solution has been diluted by cold water. Based upon this reasoning, quartz saturation temperatures were plotted versus the concentration of chloride for available groundwater analysis in the Central Sevier River Valley. Chloride concentration was chosen as an index of dilution because it is independent of most mineral equilibria and is not subject to complexing at moderate temperatures and ionic strengths. The analyses reported by Young & Carpenter (1965) for flowing springs and wells in the area contain values for dissolved silica for Red Hill and Monroe Springs which are 40 percent higher than those measured by our analysis. On this evidence these analyses were presumed to contain erroneously high

dissolved silica values. However, it was assumed that these analyses were internally consistent and could, therefore, be meaningfully compared relative to one another. Silica versus chloride plots of these data are presented in figure 12. The low chloride solutions are greatly dispersed, but a tight cluster, represented by open circles, can readily be distinguished. This group has an average quartz saturation temperature of  $85^{\circ}$  centigrade and average pH of 7.5. Joseph Hot Springs, with the highest chloride concentration in the population, has a quartz saturation temperature of  $128^{\circ}\text{C}$  and pH of 6.6. Three high chloride analyses, including Red Hill Spring, plot linearly between these two points. These points are represented by closed triangles. The Red Hill and Joseph Hot Springs would appear to be the result of mixing of high and low temperature fluids. Fifty percent dilution of Joseph Hot Springs water is required to produce the Red Hill Spring chloride concentration and quartz saturation temperature.

Despite the strong suggestion that the Red Hill Spring water represents a more dilute source fluid than the Joseph Spring water, it is obvious that both have completely re-equilibrated with respect to calcite at their present spring temperatures and pH's. The fact that the Red Hill Spring is saturated with respect to quartz while the Joseph Hot Spring is apparently supersaturated, suggests that the former contains water that has risen much more

Figure 12. Chloride and silica content of wells and  
springs in the Central Sevier River Valley.



rapidly from the site of mixing, such that it has not cooled significantly. This is a reasonable assumption since the Red Hill Spring has a much greater rate of flow than the Joseph Hot Spring.

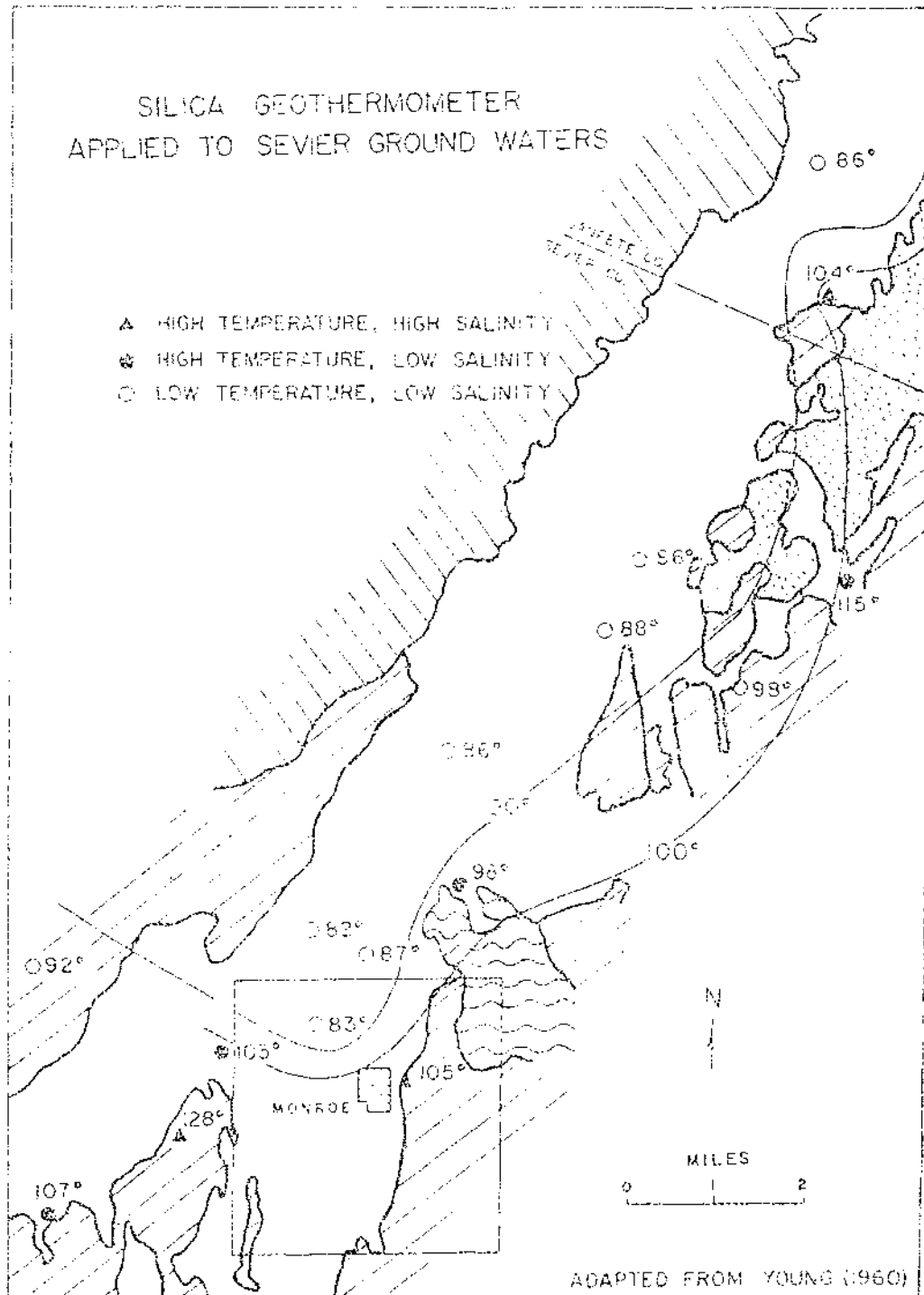
The quartz saturation temperatures, calculated from the analyses reported by Young, have been plotted on a map of the Central Sevier River Valley (figure 13). Also indicated are different groundwater populations as identified by the mixing plot (figure 13). The map clearly shows a ridge of high silica temperatures which follows the edge of the Sevier Plateau and then bends westward south of Monroe following the shoulder of the Antelope Range anticline. The high chloride warm springs (closed triangles) outcrop along this ridge as do also low chloride waters with anomalously high quartz saturation temperatures (closed circles). Low chloride waters with quartz saturation temperatures approximating  $85^{\circ}\text{C}$  outcrop along the valley floor (open circles). Low chloride waters with quartz saturation temperatures below  $70^{\circ}\text{C}$  have no clear spatial distribution and are considered to be derived from aquifers which have no importance to the proposed mixing model. These solutions are represented by crosses on figure 12.

On the basis of this evidence two sources of the spring water are proposed. A high temperature, sulfate dominated fluid is hypothesized which has high salinity and low pH. It may be derived from a deep thermal reservoir

Figure 13. Quartz saturation temperatures for wells and springs of the Central Sevier River Valley.

# SILICA GEOTHERMOMETER APPLIED TO SEVIER GROUND WATERS

- ▲ HIGH TEMPERATURE, HIGH SALINITY
- ⊙ HIGH TEMPERATURE, LOW SALINITY
- LOW TEMPERATURE, LOW SALINITY



Tertiary Volcanics
  Tertiary Sediments
  Anapian Shale
  Quaternary Landslide

ADAPTED FROM YOUNG (1960)

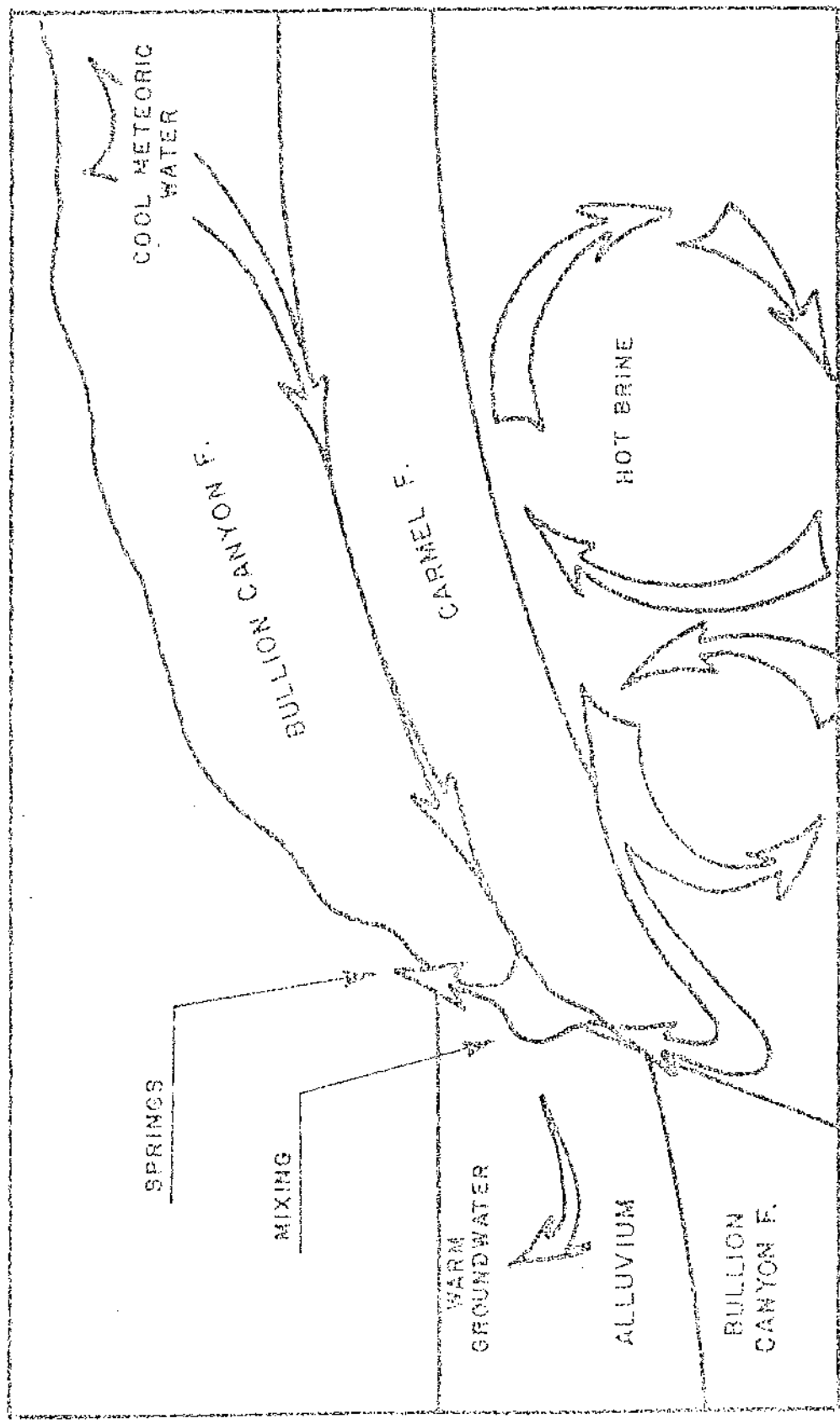


although this cannot be determined. The Red Hill and Joseph Hot Springs represent fluid derived from this source which has mixed with groundwaters of the type which outcrops along the valley floor, namely low salinity warm water with neutral pH's. Certain of the high silica, low chloride waters which outcrop near the hot springs may represent solutions derived from this same aquifer but which have been heated in the anomalously high geothermal gradient accompanying the range front. It is proposed that mixing may occur in the vicinity of the Carmel shales which serve as an impermeable boundary between hot and cold aquifers until they encounter fractures associated with the range front fault system (figure 14).

If mixing, followed by redistribution of the major ions via equilibrium with carbonate and sulfate minerals, does account for the present spring water, the Na-Ca-K geothermometer may provide an erroneous estimate of reservoir temperatures. Curiously, however, Na-Ca-K temperatures estimates do reproduce the thermal anomaly observed when quartz saturation estimates were mapped (figure 13). High Na-Ca-K temperatures for the warm springs may result if  $K^+$  is concentrated in the high temperature brine. Under these conditions Na-Ca-K temperatures should be negatively correlated with the dilution of the high temperature brine.

A few boundary conditions can be placed upon a hypothetical high temperature source fluid. It is not likely that the Joseph Spring represents an undiluted high

Figure 14. Proposed model for the Monrce Hot Springs.



temperature fluid. Rather, it probably represents a point on the dilution curve along with the Red Hill Spring. Therefore, the temperature of the fluid must exceed the quartz saturation temperature of the Joseph Hot Spring. Unfortunately, this value is not accurately known at the time of this writing. Based upon the apparent 40 percent overestimation of the silica activity in the analyses reported by Young and Carpenter, it is probably greater than 90°C.

When water is hypothetically equilibrated with calcite and gypsum at a pH of 6.6, at temperature of 70°C and a NaCl molality of .025, an activity of sulfate lower than that observed in the hot springs is obtained. It was therefore assumed that the composition of the hot springs must be controlled by sulfate introduced from outside the Carmel shales. Calculations revealed that an initial activity of that ion equal to .0025 will result, after equilibration with calcite and gypsum, in a sulfate activity of .0035, equivalent to that of Red Hill Spring. This value represents a minimum for the mixed solution before equilibrium with carbonate rocks. Therefore, it seems likely that the hot source fluid contains elevated sulfate and that this sulfate is derived from the oxidation of dissolved sulfide.

#### Heat Flow

A model has been proposed for the Monroe Spring system

in which deep, convecting high temperature brines are confined beneath the impermeable Carmel shale. Low temperature groundwaters are presumed to recharge in the uplands of the Sevier Plateau and to flow through the Tertiary volcanic formations following the dip of the Sevier monocline. The two solutions mix in the vicinity of the Monroe Springs where the impermeable shale is interrupted by the Sevier range-front fault system (figure 14).

It is assumed that heat transfer in the Monroe thermal system is due to convection below the Carmel shale and conduction above. Convective heat transfer attending circulation of hot spring waters in the Sevier fault system is considered to be insignificant. The convecting cell is assumed to be large enough such that the heat flow can be estimated by a one-dimensional model.

The minimum estimated temperature for the upper part of the convective system is  $100^{\circ}\text{C}$  based upon the mixing model. The maximum thickness of the Bullion Canyon volcanic formation which overlies the shale is 1.2 km. The total depth to the base of the Carmel shale is estimated at 1.8 km. Therefore, a minimum thermal gradient of  $47^{\circ}\text{C}/\text{km}$  is expected over the convecting thermal solutions in the Sevier Plateau uplands. This is roughly twice the normal thermal gradient of  $27^{\circ}\text{C}/\text{km}$  measured by the University of Utah in the Bullion Canyon volcanics eight miles southwest

of Monroe (T26S/R3W/Sect.3).

Along the range front the depth to the base of the Carmel shale is estimated at 1 km. This results in a thermal gradient of  $85^{\circ}\text{C}/\text{km}$  or roughly three times the normal gradient. Topographic corrections were not included in the calculations, nor were the effects of groundwater circulation in the Tertiary volcanics considered. The effect of the latter would be to decrease the thermal anomaly associated with the proposed convective cell in the uplands and to increase the heat flow in the valley.

Groundwaters which have their area of recharge in the plateau uplands might be expected to circulate to the depth of the Carmel shale horizon. If a thermal gradient of  $47^{\circ}\text{C}/\text{km}$  is assumed for this terrain, the minimum temperatures that can be expected for the Sevier Valley groundwaters are in the range of  $55^{\circ}\text{C}$ . This is in excellent agreement with the quartz saturation temperatures estimated for the Central Sevier River Valley groundwaters based upon the analysis reported by Young and Carpenter (1965).

## ALTERATION GEOCHEMISTRY

The surficial alteration observed in the Monroe KGRA should reflect the chemistry of the altering hydrothermal fluids. The advanced argillic zone represents the most intense surficial alteration. It is assumed that the phases in this zone most accurately reflect the properties of the source solutions and that solutions capable of generating the typical argillic and propylitic assemblages have been derived from these source solutions as a consequence of fluid-rock reactions.

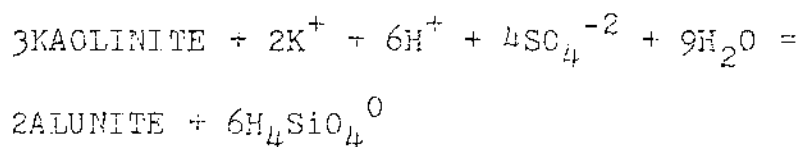
Theoretical activity diagrams depicting the stability relationships among the principle phases at various temperatures and solution compositions were constructed using thermodynamic data contained in Helgeson (1969), tables 3, 7, 8, 11 and 12 and Kelley and Shomate (1946). The pertinent thermodynamic constants are reported in table 6. Alunite has been incorporated in the diagrams in place of jarosite because the alunite-kaolinite reaction is better understood than the jarosite-kaolinite reaction, because heat capacity data is not available for jarosite, and because of the difficulties introduced by uncertainties in  $Fe^{+3}$  activities. The  $\log(a_{Fe^{+3}}/a_{Al^{+3}})$  ratios required to stabilize jarosite over alunite are moderate, 1.7 at

Table 6. Thermodynamic data

	STANDARD ENTHALPY 298°K	STANDARD ENTROPY 298°K	AVERAGE HEAT CAPACITY			HEAT CAPACITY FUNCTION		
			60°	100°	150°	a	b $\times 10^3$	c $\times 10^{-5}$
Natural alunite	-1235600 cal.	76.1 cal.				231	78.6	-67.8
crystalline gibbsite	-357180 cal.	28.02 cal.				8.65	45.6	
kaolinite	-980020 cal.	48.53 cal.				67.9	19.2	-13.7
microcline	-946000 cal.	52.47 cal.				63.8	12.9	-17.1
Ca-montmorillonite	-1367930 cal.	61.2 cal.				84.2	33.6	-20.0
muscovite	-1420900 cal.	69.0 cal.				97.6	26.4	-25.4
H <sub>4</sub> SiO <sub>4</sub>	-348060 cal.	45.84 cal.	49	49	46			
H <sup>+</sup>	0 cal.	0 cal.	23	31	33			
H <sub>2</sub> O	-68315 cal.	16.71 cal.	18	18	18			
Ca <sup>-2</sup>	-129770 cal.	-13.2 cal.	45	59	60			
K <sup>+</sup>	-60040 cal.	24.5 cal.	27	35	35			
SO <sub>4</sub> <sup>-2</sup>	-217320 cal.	4.8 cal.	-99	-108	-105			



25°C, if the free energy of jarosite reported by Brown (1970) is used. These values are probably attained locally in response to the dissolution of ferromagnetism aluminosilicates. The theoretical free energy for the reaction:



probably represent an upper bound. Raymahashay (1968) demonstrated a lower free energy for this reaction in natural hot springs. Furthermore, under conditions of low temperature and intermediate acidity where the crystallization rate of silicates to non-silicates are very low, "it is conceivable that alunite may be produced well outside of its stability field in the breakdown of feldspathic rock by sulfate solutions" (Brown, 1969). Therefore, the size of the alunite field presented in the diagrams should be considered a practical minimum.

Ca-montmorillonite was included instead of K-montmorillonite since that mineral does not form in the alteration assemblages and since the size of the montmorillonite field would be underestimated otherwise. Since gypsum is a common mineral in advanced argillic assemblages,  $\text{Ca}^{+2}$  activities were chosen to be the saturation value with respect to gypsum for any given  $\text{SO}_4^{-2}$  activity and temperature.

Owing to the difficulties inherent in estimating the

activities of aluminum species, all reactions were written to conserve aluminum.

Two types of diagrams were calculated. The first is a three-dimensional presentation of the stability relationships among the phases as a function of log potassium, sulfate and hydrogen ion activities. These diagrams are particularly attractive because they include, indirectly, the effects of  $fH_2S$ . Saturation with respect to both gypsum and quartz is assumed.

The most striking feature of these diagrams is the sensitivity of the kaolinite volume to temperature. Above  $150^{\circ}C$  the kaolinite volume is almost entirely displaced by that of montmorillonite (figure 15). Since one of the important characteristics of the argillic and advanced argillic zone is abundant and often massive kaolinite, this is taken as evidence that the altering solutions must not have exceeded  $150^{\circ}C$ .

Another important observation is that alunite is stable with respect to the other phases at moderate pH's and ion activities. In figure 16 horizontal planes through the diagram at pH five and six show the range of sulfate and potassium concentrations in equilibrium with alunite for the given pH values. At a pH of five the alunite field intersects the composition of the Red Hill Spring water. It is therefore apparent that the presence of jarosite in the advanced argillic zone does not necessarily indicate that

Figure 15. Stability relations among the phases alunite, kaolinite, Ca-montmorillonite and microcline at 150°C for solutions saturated with respect to gypsum and quartz.

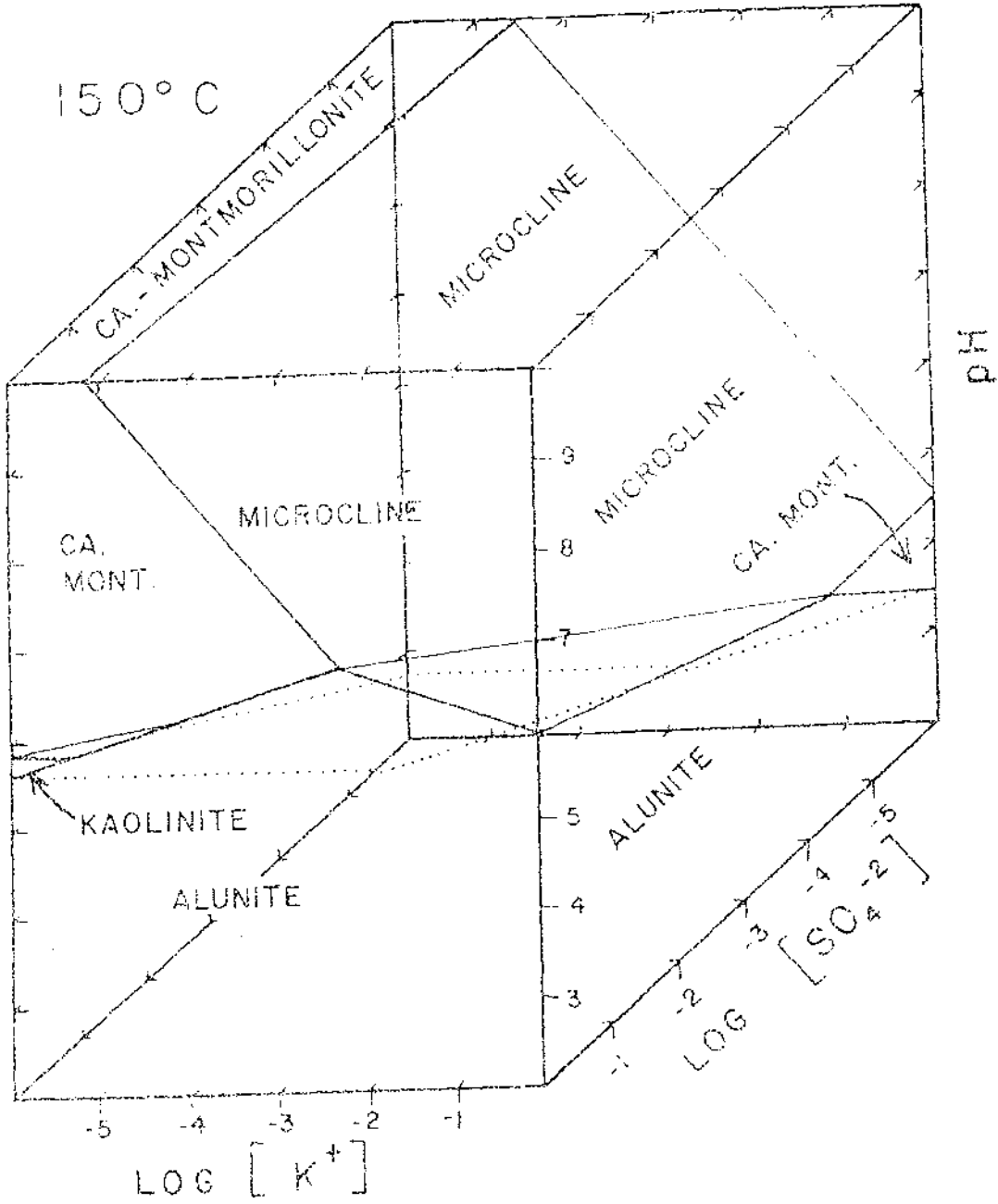
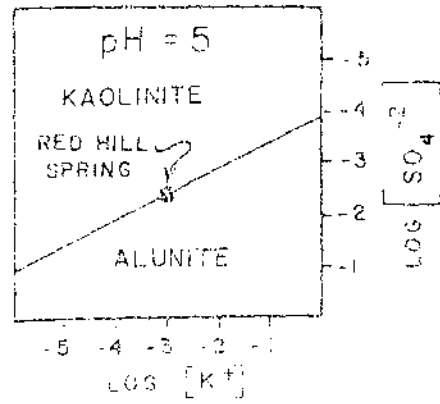
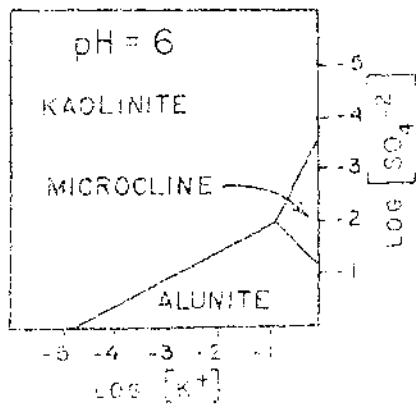
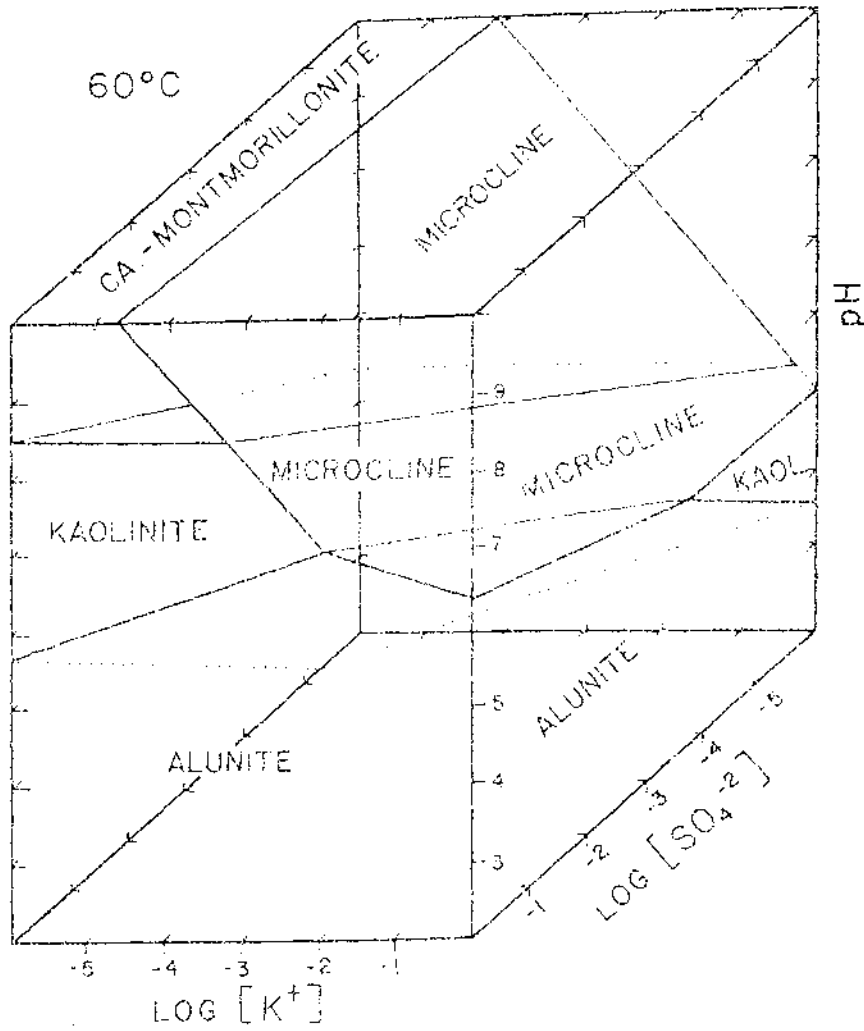


Figure 16. Stability relations among the phases alunite, kaolinite, Ca-montmorillonite and microcline at 60°C for solutions saturated with respect to gypsum and quartz.



the altering solutions were highly acidic.

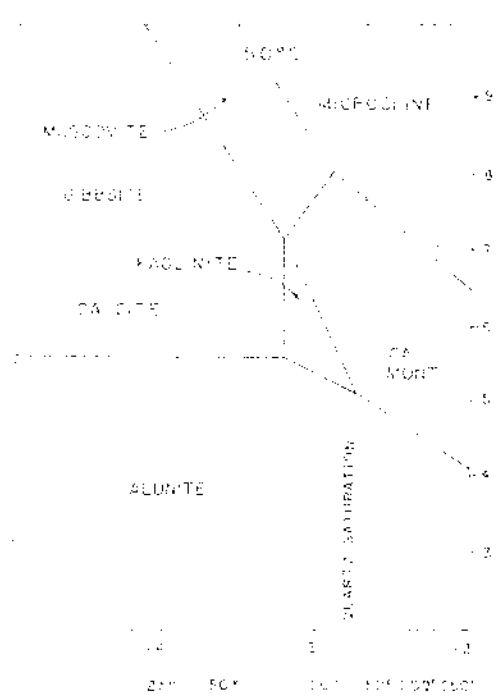
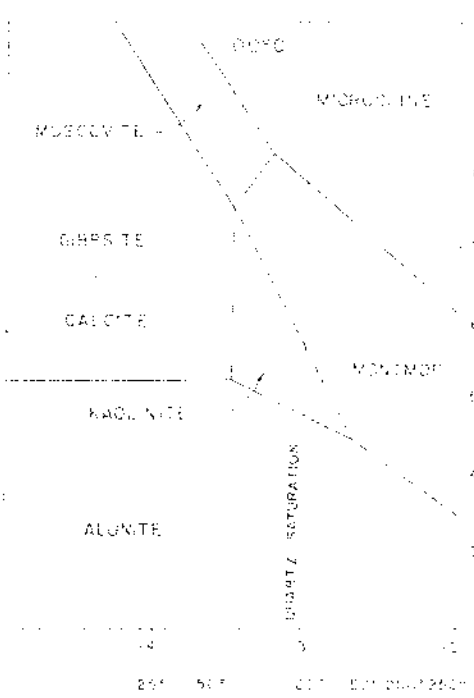
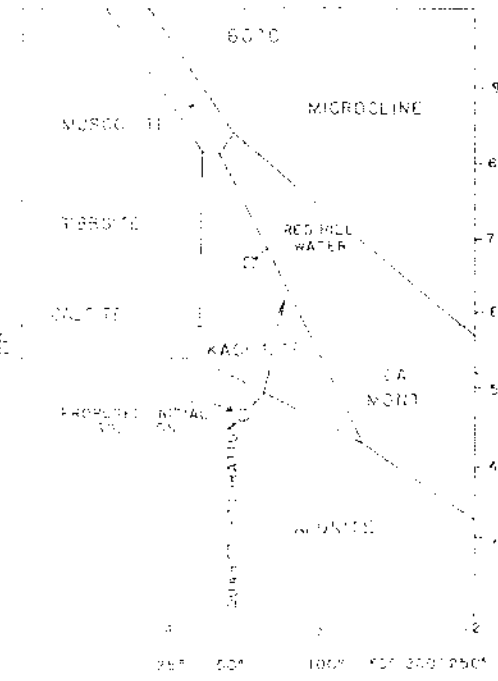
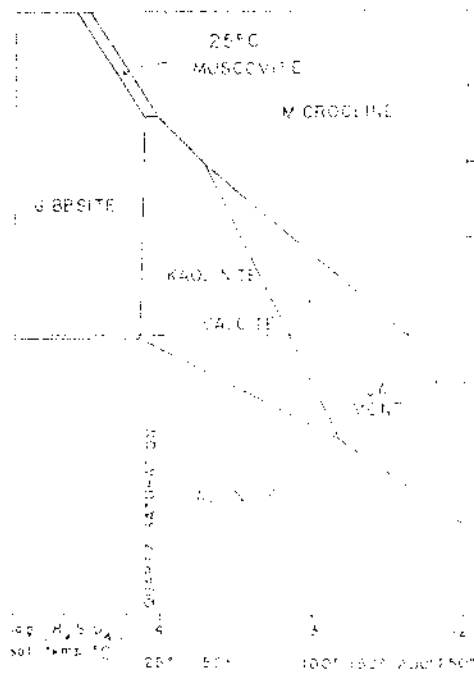
At a  $f\text{CO}_2$  of four, approximately equivalent to saturation at a depth of 150 feet if a hydrostatic pressure gradient is assumed, calcite first intersects the alunite volume for a temperature of  $60^\circ\text{C}$ . However, greater pressures, corresponding to depths exceeding 500 feet are required to precipitate calcite with alunite at reasonable ion activities.

A series of isothermal diagrams were also calculated using the activities of silica and pH as the independent variables (figure 17). These diagrams correspond to vertical lines through the three dimensional diagrams at the potassium and sulfate concentrations of the Red Hill Spring, considered to represent a minimum estimate for the hydrothermal solutions.

It is assumed that the silica concentrations of the solutions will never fall below the quartz saturation values, provided quartz is a participating phase. This assumption is supported by the observation that secondary polycrystalline quartz occasionally forms as a pseudomorph after ferromagnesium aluminosilicates. On the other hand, supersaturation with respect to quartz is likely, provided the solutions have cooled following last wall rock equilibration. The diagrams may be visualized as depicting the reaction of various source solutions possessing quartz saturation temperatures ranging between the saturation value for a particular diagram and a practical maximum,  $275^\circ\text{C}$ .

Figure 17. Stability relations among the phases alunite, kaolinite, gibbsite, Ca-montmorillonite, muscovite and microcline as a function of temperature, pH and silica concentration. Saturation with gypsum is assumed. The calcite saturation line is shown for a  $PCO_2$  of four atmospheres. The solution path is shown for the reaction of the proposed initial solution with potassium feldspar.





For this reason the silica concentrations have been reported both in terms of molalities and in terms of the corresponding quartz saturation temperature.

Regardless of the temperature at which the reactions are calculated, kaolinite cannot form stably if the solutions entering into the reactions have equilibrated with quartz at temperatures above  $150^{\circ}\text{C}$ . Therefore a maximum limit on the mixing temperature of  $150^{\circ}\text{C}$  is established. The kaolinite field would, of course, be enhanced at higher temperatures if lower ion activities than those at the Red Hill Spring are chosen. It is unlikely that this would represent a realistic situation, however.

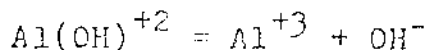
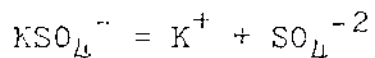
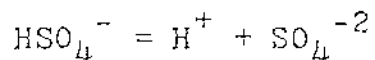
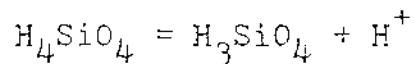
The intersection of the kaolinite-Ca montmorillonite field boundary with the quartz saturation line falls below the calcite field boundary at temperatures of  $100^{\circ}\text{C}$  and above. This means that for calcite and kaolinite to coexist, temperatures below  $100^{\circ}\text{C}$  are required. Since these two minerals are commonly associated, the near surface reaction temperatures have probably remained below  $100^{\circ}\text{C}$  during most of the history of the area.

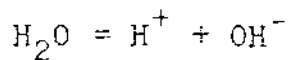
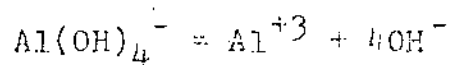
The difficulty of precipitating muscovite is apparent. It is most likely to precipitate at lower temperatures where the quartz saturation line approaches the muscovite field and at neutral pH's. It may form at high temperatures provided the reactions are confined to a silica deficient environment. This observation is in good agreement with

the lack of extensive sericite replacement in the KGRA. The stability field of mixed layer potassium micas has not been estimated. However, it would certainly encroach significantly on both the kaolinite and montmorillonite fields, making it an easily attainable phase.

The sequence of hydrothermal alteration observed at Monroe could have been generated by hydrothermal solution not unlike the present spring waters. An initial solution composition approximating that of the present springs with a temperature of 60°C and a pH of five is proposed. Particularly if the source solution is more concentrated in sulfate and potassium than the present springs an initial pH of five is more than sufficient to account for the occurrence of jarosite in the innermost advanced argillic zone.

The theoretical solution path for the reaction of the proposed initial solution with potassium feldspar has been plotted in figure 17. The path was calculated using the mass transfer algorithm described by Helgeson et al., (1969). The following partial equilibria were included in the calculation:





Quartz was not included as a product mineral in the reaction matrix.

The solution path moves first into kaolinite field and then to the montmorillonite-kaolinite field boundary, generating argillic and propylitic alteration assemblages respectively. Calcite coexists with kaolinite as a pH of approximately six is reached. The concentrations of  $\text{K}^+$  and  $\text{SO}_4^{-2}$  are not significantly affected by the reaction.

Muscovite or sericite may precipitate as late phases, produced by spent hydrothermal fluids with low temperatures and hydrogen ion activities. Superimposition of different alteration assemblages occurs as the hydrothermal system cools and contracts. Gypsum as a replacement of jarosite could have formed as the advanced argillic regime was superceded by an argillic regime in which jarosite was not stable.

The peculiar association of alunite and jarosite with minor calcite at Goldfield, Nevada and Monroe respectively is probably a metastable relationship. The volume of calcite is small in both cases. Furthermore, owing to the fact that only very small variations in pH, less than one log unit, are sufficient to move from the stability field of alunite or jarosite into that of kaolinite and calcite, it is surprising that these associations are not more common.

The formation of chlorite appears to represent a special case. Chlorite always forms in close association with biotite but never as a replacement product. Therefore, chlorite must form from solutions that are in partial equilibrium with biotite.

The initial solutions appear to have high potassium activities. For this reason calcium phases are consumed preferentially and potassium feldspar and sericite may persist metastability (Fournier and Truesdall, 1973). However, as  $\text{Ca}^{+2}$  activity rises in response to the consumption of sulfate, these phases are also consumed.

## CONCLUSION

The Monroe KGRA represents the peripheral oxidized zone of an active sulfide containing system. The near surface environment represented by the exposed alteration is consistent with sulfate solutions with temperatures between 50° and 150°C. Moderate pH's of five or greater are sufficient to account for the advanced argillic alteration regime. The overall abundance of calcite suggests that high partial pressures of carbon dioxide, generated by reaction of hydrothermal solutions with sedimentary carbonates, has been an important aspect of the system over its entire history.

The spring water is consistent with the alteration found in the KGRA. Its relationship to the other springs and wells in the vicinity suggest that it is a high temperature brine which has been diluted by cool nonsaline groundwaters. The source brines must exceed 100°C and have high concentrations of sodium chloride, sulfate and potassium.

A model is proposed for the system whereby hot thermal brines are heated at depth and circulate beneath the impermeable Carmel shales. Meteoric water entering the groundwater system on the Sevier Plateau descends the Sevier

monocline through permeable volcanic rock and is slightly heated by the thermal gradient. The two solutions mix at the site of the springs where major faults interrupt the impermeable cap rock. The temperature of mixing has never exceeded  $150^{\circ}\text{C}$  but much higher temperatures are possible for the undiluted brines.

The mixed solutions equilibrate with carbonate rock before ascending to the surface. The alteration which has been produced by these fluids exhibits an inner jarosite-kaolinite zone which passes outward to kaolinite-mixed layer clay and montmorillonite-mixed layer clay zones.

APPENDIX

DATA FROM BULK ROCK AND CLAY FRACTION X-RAY DIFFRACTION AND THIN SECTION EXAMINATION  
PERCENT PATTERN INTENSITY

<u>SPECIMEN</u> <u>NO.</u>	<u>QTZ</u>	<u>PLAG</u>	<u>ORTH</u>	<u>CAL</u>	<u>DOL</u>	<u>HEM</u>	<u>JAR</u>	<u>TYP</u>	<u>AP</u>	<u>BIOT</u>	<u>KAOL</u>	<u>MONT</u>	<u>CHL</u>	<u>MIXI</u>	<u>MIXXI</u>
1 III W	37.0	37.0	6.0	12.0		1.0			1.0	2.2	0.7	2.2			
6 II	68.0		9.0			1.0	7.0	2.0		1.0	15.0				
13 I	47.0	33.0	2.0	1.0	6.0	1.0			1.0	3.7	4.0	2.6	1.7		
13 II	58.0		23.0			1.0	7.0	2.0	1.0		8.4				0.6
39	71.0					1.0	4.0	6.0			16.7			2.3	
100 II	67.0			7.0	14.0	1.0					11.0				
123	46.0	20.0	1.0	10.0	10.0	6.0				1.0	8.4	0.6			
142	67.0		18.0				3.0	1.0			10.8	0.3			
144 II	56.0	23.0	11.0			7.0				0.2	1.1	1.7			
148	33.0	43.0	16.0	1.0		1.0			1.0	4.0	0.8	4.1			
149	75.0						6.0				15.6				3.4
154	44.0	15.0	2.0	12.0	6.0	6.0				1.8	12.9				1.5
173 G	76.0		2.0			8.0	1.0			2.1	5.8		0.2		1.8
173 W	81.0		2.0			1.0	3.0			1.6	11.0		0.1		1.3



<u>SPECIMEN</u> <u>NO.</u>	<u>QTZ</u>	<u>PLAG</u>	<u>ORTH</u>	<u>CAL</u>	<u>DOL</u>	<u>HEM</u>	<u>JAR</u>	<u>TYP</u>	<u>AP</u>	<u>BIOT</u>	<u>KAOL</u>	<u>MONT</u>	<u>CHL</u>	<u>MIXI</u>	<u>MIXXI</u>
184	50.0		22.0				1.0			3.3	20.2	3.0			
187 I	65.0					9.0				1.0	26.0				
188	41.0	32 0	10.0	8.0		4.0				1.3	1.3	3.5			
302	57.0	37.0				4.0				1.0	0.4	9.0			

DATA FROM BULK ROCK AND CLAY FRACTION X-RAY DIFFRACTION  
PERCENT PATTERN INTENSITY

<u>SPECIMEN</u> <u>NO.</u>	<u>QTZ</u>	<u>PLAG</u>	<u>ORTH</u>	<u>CAL</u>	<u>DOL</u>	<u>HBM</u>	<u>JAR</u>	<u>GYP</u>	<u>AP</u>	<u>BIOT</u>	<u>KACL</u>	<u>WONT</u>	<u>CHL</u>	<u>MIXI</u>	<u>MIXII</u>
22	59.0				27.0	1.0					11.5		0.1	0.4	
51	55.0	33.0		4.0							5.7		2.7		0.6
100 I	62.0		16.0				1.0				20.0				
101	74.0		2.0		11.0						14.0				
125	54.0	17.0		3.0	16.0					1.1	8.2	0.3	0.1		0.3
174	69.0		6.0	2.0			2.0				19.1		0.2		1.7
175 II	66.0		11.0			2.0					15.7			6.1	
181	57.0	13.0	5.0			5.0		1.0		0.9	6.3	5.0		1.2	
189	51.0			31.0	3.0						12.6				2.4
190 I	50.0	38.0									9.9			1.6	
300	53.0	23.0	4.0	1.0			1.0			1.0	15.7		1.2		1.8
305	20.0	38.0	38.0							0.2		0.5		3.8	

DATA FROM BULK ROCK X-RAY DIFFRACTION AND THIN SECTION EXAMINATION  
PERCENT PATTERN INTENSITY

SPECIMEN NO.	QTZ	PLAG	ORTH	CAL	DOL	HEM	JAR	GYP	AP	BIOT	KAOL	MONT	CHL	MIXI	MIXII
1 III G	47.0	33.0	1.0	7.0		8.0				4.0					
14	46.0	39.0	1.0	12.0							1.0				
16	45.0	20.0	1.0		30.0	1.0				2.0	4.0				
19	69.0	25.0	1.0			1.0					6.0				
26	55.0	44.0	1.0			4.0				1.0					
82 I	62.0	11.0	1.0	14.0		7.0				1.0	5.0				
82 II	65.0	26.0	1.0			1.0				3.0	3.0				3.0
94 I	66.0	20.0	1.0			9.0				1.0	2.0				
94 II	45.0	52.0	1.0	1.0		1.0				1.0	1.0				
112	56.0	31.0	8.0			5.0				1.0		1.0			
128	35.0	53.0	7.0	1.0		4.0				1.0					
129	33.0	18.0		44.0	2.0	1.0				1.0	2.0				
145	53.0	35.0	7.0				4.0	1.0		1.0					

<u>SPECIMEN NO.</u>	<u>QTZ</u>	<u>PLAG</u>	<u>CRTH</u>	<u>CAL</u>	<u>DOL</u>	<u>HEM</u>	<u>JAR</u>	<u>GYP</u>	<u>AP</u>	<u>BIOT</u>	<u>KAOL</u>	<u>MONT</u>	<u>CHL</u>	<u>MIXI</u>	<u>MIXII</u>
152	63.0	13.0	2.0	8.0	9.0			1.0		1.0	4.0				
155	65.0		4.0			1.0	7.0	1.0			18.0				4.0
158	40.0	40.0	4.0	2.0	8.0	5.0									
175 I	50.0	8.0	3.0	28.0		7.0				2.0	2.0				
190 III	42.0	42.0			12.0	1.0					3.0				
192 I	56.0	11.0	11.0	1.0	11.0	1.0				2.0	1.0				
192 II	68.0	18.0	9.0			1.0			1.0	3.0	2.0				
197 I	51.0	35.0				7.0				4.0					
202	55.0	37.0	1.0	3.0		3.0					1.0	2.0			
205 I	62.0	24.0				6.0				4.0	4.0				
205 II	72.0	20.0				1.0				1.0	6.0				
216	36.0	38.0	1.0			7.0				9.0	1.0				
232	10.0	80.0		5.0		5.0									
303	30.0	59.0	10.0							2.0					
308	42.0	42.0	12.0			4.0									

DATA FROM BULK ROCK X-RAY DIFFRACTION  
PERCENT PATTERN INTENSITY

<u>SPECIMEN NO.</u>	<u>QTZ</u>	<u>PLAG</u>	<u>ORTH</u>	<u>CAL</u>	<u>DOL</u>	<u>HEM</u>	<u>JAR</u>	<u>GYP</u>	<u>AP</u>	<u>BIOT</u>	<u>KAOL</u>	<u>MONT</u>	<u>CHL</u>	<u>MIXI</u>	<u>MIXII</u>
6 I	53.0	9.0	1.0	4.0	24.0	5.0					5.0				
6 III	54.0	27.0	9.0		3.0	1.0					6.0				
20 II	57.0	37.0				4.0				1.0	1.0				
23	35.0	60.0		1.0	4.0										
24	70.0	19.0	5.0							3.0	3.0				
25	42.0	49.0	1.0		1.0	3.0	1.0				4.0				
79 I	50.0	46.0				4.0									
85	38.0	53.0		2.0		2.0				1.0	4.0				
92 II	54.0	23.0	2.0	10.0		11.0									
92 III	62.0	35.0									3.0				
93 II	52.0	36.0	1.0		1.0	5.0				1.0	2.0				
102	47.0	23.0			23.0	4.0				2.0					
118	52.0	39.0	2.0		1.0	5.0				1.0					
119	60.0	16.0	16.0			5.0				2.0					

<u>SPECIMEN NO.</u>	<u>QTZ</u>	<u>PLAG</u>	<u>ORTH</u>	<u>CAL</u>	<u>DOL</u>	<u>HEM</u>	<u>JAR</u>	<u>GYP</u>	<u>AP</u>	<u>BIOT</u>	<u>KAOL</u>	<u>MONT</u>	<u>CHL</u>	<u>MIXI</u>	<u>MIXII</u>
124 IV	36.0	54.0			2.0	8.0									
130	70.0	24.0				4.0				2.0					
138											1.0	99.0			
140	55.0	24.0		1.0	18.0					1.0	1.0				
150	38.0	36.0	10.0	4.0	10.0						2.0				
180	54.0		18.0							9.0	9.0	10.0			
183	64.0		13.0			6.0				2.0	9.0	6.0			
185	47.0	40.0		8.0							6.0				
186	39.0	41.0		10.0		2.0					2.0	5.0			
187 II	82.0									1.0	17.0				
187 III	75.00					20.0					5.0				
190 II	55.0	11.0			25.0						5.0			4.0	
191	54.0	18.0	4.0	7.0	13.0					2.0	2.0				
193 I	47.0	8.0		35.0		7.0					2.0				2.0
193 II	61.0	29.0			1.0	6.0				2.0					
193 IV	76.0	8.0				2.0					7.0				7.0
194 I	72.0	11.0	11.0								6.0				

SPECIMEN NO.	QTZ	PLAG	ORTH	CAI.	DOL	HEM	JAR	GYP	AP	BIOT	KAOL	MONT	CHL	MIXI	MIXII
194 II	45.0	29.0	8.0	15.0							2.0				
212	41.0	50.0				9.0									
220	7.0	47.0	47.0												
221	38.0	30.0	30.0			2.0									
231		50.0	50.0												

## REFERENCES

- Berner, R. A., 1969, Geothite Stability and the Origin of Red Beds: *Geochimica et Cosmochimica Acta*, v. 33, p. 267.
- Brown, J. B., 1970, A Chemical Study of some Synthetic Potassium-Hydronium Jarosites: *The Canadian Mineralogist*, v. 10, p. 696.
- Brown, J. B., 1971, Jarosite-Geothite Stabilities at 25°C, 1 Atm.: *Mineralium Deposita (Berl)*, v. 6, no. 3, p. 245.
- Callaghan, Eugene, 1938, Preliminary Report on the Alunite Deposits of the Marysvale Region, Utah: U. S. Geologic Survey Bulletin, no. 886-D.
- Callaghan, Eugene, and Thomas, Harold, 1939, Manganese in a Thermal Spring in West-Central Utah: *Economic Geology*, v. 34, no. 8, p. 905.
- Callaghan, Eugene, 1939, Volcanic Sequence in the Marysvale Region in Southwest Central Utah: *American Geophysical Union Transaction (EOS)*.
- Callaghan, Eugene, and Parker, Raymond, 1961, Geologic Map of the Monroe Quadrangle, Utah: U. S. Geological Survey.
- Carroll, Dorothy, 1970, Clay Minerals: A Guide to Their X-ray Identification: Geological Society of America, Special Paper 126.
- Davis, John, 1973, *Statistics and Data Analysis in Geology*: New York, John Wiley and Sons, Inc.
- Fournier, R. O. and Truesdell, A. H., 1973, An empirical Na-K-Ca geothermometer for natural waters: *Geochim. et. Cosmochim. Acta*, v. 37, p. 1255-1276.
- Fournier, R. O., White, D. E., and Truesdell, A. H., 1974, Geochemical indicators of subsurface temperature - Part 1, Basic assumptions: *Jour. Research U. S. Geol. Survey*, v. 2, p. 259-262.



- Fournier, R. O., and Truesdell, A. N., 1974, Geochemical indicators of subsurface temperature - Part 2, Estimation of temperature and fraction of hot water mixed with cold water: Jour. Research U. S. Geol. Survey, v. 2, p. 263-270.
- Garrels, Robert, and Christ, Charles, 1965, Solutions, Minerals and Equilibria, San Francisco, Freeman, Copper and Co.
- Hardy, C. T., 1952, Eastern Sevier Valley, Sevier and Sandpete Counties, Utah: Utah Geological and Mineralogical Survey, Bulletin 43, p. 98.
- Helgeson, Harold C., Brown, Thomas H., Nigrini, Andrew, Jones, Thomas A., 1969, Mass Transfer in Geochemical Processes Involving Aqueous Solutions: Geochimica et Cosmochimica Acta, v. 34, p. 569.
- Hemley, J. J., and Hostetler, P. B., Gude, A. J., et al., 1969, Some Stability Relations of Alunite: Economic Geology, v. 64, no. 6, pp. 599.
- Kelley, K. K., Chomate, C. H., et al., 1946, Thermodynamic Properties of Potassium Alum and Related Substances with Reference to Extraction of Alumina from Clay and Alunite: U. S. Bureau of Mines Technical Paper, no. 688.
- Mundorff, J. C., 1970, Major thermal springs of Utah: Utah Geological and Mineralogical Survey Water-Resources Bulletin 13, 60 p.
- Nriagu, Jerome, 1971, Expressions for Calculating the Soluabilities of Metal Sulfides in Hydrothermal Solutions: Canadian Journal of Earth Sciences, v. 8, p. 813.
- Presser, T. S. and Barnes, Ivan, 1974, Special Techniques for Determining the Chemical Properties of Geothermal Water: NITIS, U. S. Department of Commerce, PB-235 148, p. 11.
- Ransome, F. L., et al., 1909, The Geology and Ore Deposits of Goldfield, Nevada: U. S. Geologic Survey, Professional Paper 66.
- Raymahashay, B. C., 1968, A Geochemical Study of Rock Alteration by Hot Springs in the Paint Pot Hill Area, Yellowstone Park: Geochimica et Cosmochimica Acta, v. 32, p. 499.

Sneath, P. H. and Sokal, R. R., 1973, Numerical Taxonomy:  
The Principles of Numerical Classification: San  
Francisco, W. H. Freeman.

Young, Richard A. and Carpenter, Carl H., 1965, Groundwater  
Conditions and Storage in the Central Sevier Valley,  
Utah: U. S. Geological Survey Water-Supply Paper,  
no. 1787.

## VITA

Name Charles David Miller

Birthplace Fort Collins, Colorado

Birthdate August 9, 1951

High School Garden Spot High School  
New Holland, Pennsylvania

College 1969-1973 The College of William and Mary  
Williamsburg, Virginia

University 1974-1976 University of Utah  
Salt Lake City, Utah

Degree B.S. in chemistry  
The College of William and Mary  
Williamsburg, Virginia

Publications Parry, W. T., Benson, Nancy and  
Miller, Charles D., 1976, Geochemistry  
and Hydrothermal Alteration at  
Selected Utah Hot Springs: Final  
Report on Grant No. GI-43741,  
National Science Foundation, vol. 3.

DeVries, G. H., Mamunes, P., Miller,  
C. D., and Hayward, D. M., 1976,  
Quantitative Determination of C (6:0) -  
C (18:3) Serum Nonesterified Fatty  
Acids by Gas-Liquid Chromatography:  
Analytical Biochemistry 70, 156-166.

Mamunes, P., DeVries, G. H., Miller,  
C. D., and David, R. B., 1975, Fatty  
Acid Quantitation in Keyes Syndrome:  
Keyes Syndrome (J. D. Pollack, ed.)  
pp. 245-254, Grune and Stratton, New  
York.